UTILIZING FUNCTIONALIZATION TO ACCESS ADVANCED MATERIALS PROPERTIES

Anne-Martine S. Jackson

A dissertation submitted to the faculty of the University of North Carolina at Chapel Hill in partial fulfillment of the requirements for the degree of Doctor of Philosophy in the Department of Chemistry

Chapel Hill
2014

Approved By:

Valerie S. Ashby

Sergei S. Sheiko

Wei You

David Nicewicz

René López

ABSTRACT

Anne-Martine S. Jackson: Utilizing Functionalization to Access Advanced Materials Properties
(Under the direction of Valerie S. Ashby)

While there are many materials that can perform a single selected task very well, there is a growing need for smart materials to advance technology in a variety of fields. Smart materials are often inspired by complex biological systems, and thus need to respond to external stimuli and perform multiple functions. It is desired that these materials have the ability to respond to changes in temperature, pressure, pH, light, magnetic field and the presence of other chemicals. A few of the functions that these materials are to perform include sensing, actuating, self-healing, recognition, self-cleaning, and optical switching. To produce materials with the range of tasks that are needed, new and elegant ways to integrate functionality into polymeric systems are needed.

Functionality can be integrated into existing polymers either chemically or physically. When modifying an existing polymer chemically, the chemical functionality as well as the placement needs to be considered. The same chemical moiety integrated either into the bulk, on the surface or as an endgroup will achieve drastically different effects. Alternatively, to introduce physically functionality, a material must be able to change potential energy, topography or mechanical properties upon the application of an external stimulus. In both cases, the properties

of a material and the functions that it can perform are highly dependent on structure and the molecular functionality of the polymer.

This thesis describes the functionalization of polymeric materials via three synthetic routes, surface, bulk and endgroup functionalization, to achieve unique physical and chemical properties. Specifically, grafting of polymeric brushes was utilized to achieve simultaneous control of surface wetting and wrinkling effects (Chapter I), unique iodinated monomers were copolymerized with methyl methacrylate to achieve bulk x-ray contrast in bone cement materials (Chapter II), and aromatic polyesters were endcapped with ureidopyrimidinone moieties to achieve end-functionalized materials with variable properties (Chapter III).

ACKNOWLEDGEMENTS

I would first like to thank my advisor, Valerie, for her support and dedication to my education and future. Along the way, I have gotten a lot of help and had many thoughtful conversations with the members of my research group, and most especially Jason Rochette, Sarah Brosnan, Sara Turner and Katie Houston. In relation to the work in Chapter I, I would like to thank MIRT for funding (NSF DMR-1122483). In addition, I would like to thank Dr. Carrie Donley at CHANL for performing XPS, and Saadya Averick and Antonia Simakova at Carnegie Mellon University for their assistance in learning ARGET ATRP. The work presented in Chapter II was supported by NSF DMR-1206957. I would like to thank the two undergraduate researchers I had the pleasure of working with, Hung Nguyen and Daniel Liauw, for their hard work on the synthetic aspects of this project. The BRIC at UNC performed the CT scans to image the bone cements, and Dr. Amar Kumbhar at CHANL did EDS on the particles. For the work in Chapter III, I would first like to thank Eastman Chemical for providing funding and materials. I would also like to thank the hard work of Katie Houston for assisting with film processing and tensile testing, and Theo Dingemans for imparting some of his vast knowledge of synthesis and processing of aromatic materials.

Aside from the academic acknowledgements, I need to thank my family, friends, and Mathew Finniss for their support and keeping me sane. It's a tough job.

TABLE OF CONTENTS

LIST OF TABLES

LIST OF FIGURES

LIST OF ABBREVIATIONS

AIBN	azobisisobutyronitrile
ARGET	activators regenerated by electron transfer
ATR-FTIR	attenuated total reflectance Fourier transform spectroscopy
ATRP	atom transfer radical polymerization
$BaSO_4$	barium (II) sulfate
BPO	benzoyl peroxide
$CDCl_3$	chloroform-*d*
CH_2Cl_2	methylene chloride
CH_3CN	acetonitrile
$CHCl_3$	chloroform
CHDM	cyclohexanedimethanol
CT	X-ray computed tomography
$CuBr_2$	copper (II) bromide
$CuSO_4Ÿ5H_2O$	copper (II) sulfate pentahydrate
DBTDL	dibutyltin dilaurate
DMA	dynamic mechanical analysis
DMF	dimethylformamide
DMPT	*N,N*-dimethyl-*p*-toluidine
DSC	differential scanning calorimetry
E'	tensile storage modulus
EDS	electron dispersion spectroscopy
EtOH	ethanol

f_{IMMA}	feed ratio of IMMA
F_{IMMA}	copolymer ratio of IMMA
f_{MMA}	feed ratio of MMA
F_{MMA}	copolymer ratio of MMA
GPC	gel permeation chromatography
H_2O	water
HU	Hounsfield units
IMMA	3-iodo-2,2-bis(iodomethyl)propyl methacrylate
K_{assoc}	association constant
MeOH	methanol
MIS	2(6-isocyanatohexylaminocarbonylamino)-6-methyl-4[1H]pyrimidinone
MMA	methyl methacrylate
M_n	number-average molecular weight
M_w	weight-average molecular weight
MW	molecular weight
NMR	nuclear magnetic resonance spectroscopy
OEGMA	oligo(ethylene glycol) methacrylate
PBIB	propargyl 2-bromoisobutyrl
PBT	poly(butylene terephthalate)
PDI	polydispersity index
PDMS	poly(dimethylsiloxane)
PEB	poly(ethylene butylene)

PEGiBBr	poly(ethylene glycol) isobutyrylbromide
PET	poly(ethylene terephthalate)
PETG	glycol-modified poly(ethylene terephthalate)
PETG-UPy	Upy-functionalized PETG
PIT	poly(butylene isophthalate)
PMMA	poly(methyl methacrylate)
Poly(ODA-*co*-OA)	poly(octylene diazoadipate-*co*-octylene adipate)
SDS	sodium dilaurel sulfate
SEM	scanning electron microscopy
$Sn(Oct)_2$	tin octanoate
T_g	glass transition temperature
TGA	thermogravimetric analysis
THF	tetrahydrofuran
T_m	melting temperature
TPMA	tris[(2-pyridyl)-methyl]amine
UPy	ureidopyrimidinone
UV	ultraviolet
XPS	X-ray photoelectron spectroscopy
ZrO_2	zirconium (II) oxide

Chapter I
GRAFTING POLY(OEGMA) BRUSHES FROM A SHAPE MEMORY ELASTOMER AND SUBSEQUENT WRINKLING BEHAVIOR

1.1 Introduction

Wrinkles have long been considered undesirable in many materials applications, but recent attention has focused on utilizing wrinkling and other surface instabilities to control surface topography.[1,2] Wrinkling can create regular and repeatable surface topographies on multiple length scales, an ability accessible previously only by lithography and micromachining.[3] Wrinkled substrates have the potential for practical use as superhydrophobic surfaces,[4] dry adhesives,[5,6] optical materials,[7,8] anti-biofouling coatings,[9] microfluidic devices[10] and flexible electronics.[11] The simplicity in which wrinkled materials can be fabricated makes them attractive for applications that require large-scale fabrication of uniformly patterned surfaces.[12]

For wrinkle formation to occur, a mismatch in thermal expansion or swelling coefficients between the substrate and top layer is required. Common methods to access controlled wrinkled patterns involve depositing a high modulus thin film on a low modulus elastomeric substrate by metal deposition,[13,14] UV/ozone irradiation,[10] increasing crosslink density,[15,16] polymer film deposition[17] or grafting of a polymer brush layer.[12,18] Typically, the top layer is made of a hard material, such as metal, but soft polymer brushes allow for an orthogonal strategy as they exhibit

anisotropic mechanical properties due to finite extensibility of brush chains perpendicular to the substrate caused by in-plane steric repulsion.[19] Other advantages of polymer brushes over solid layers is that they are covalently bound to the substrate and thus resist delamination and cracking, and a large number of functional monomers can be polymerized by a variety of controlled surface-initiated polymerizations and thus impart chemical functionality to the surface.[20]

While growing polymer brushes from static substrates is well studied, growing polymer brushes from elastomeric substrates is less frequently examined, and there are only a few studies of wrinkling in elastomer-brush bilayer systems. In one example, Stafford *et al.* found they could use surface wrinkling to characterize the height and modulus of poly(methyl methacrylate) brushes grown from a post-functionalized poly(dimethylsiloxane) (PDMS) substrate.[18] In a second example, poly(2-hydroxyethyl methacrylate) and poly(oligo ethylene glycol methacrylate) (poly(OEGMA)) brushes were grown from a bulk functionalized PDMS substrate.[12]

While the vast majority of controlled wrinkling behavior is studied on PDMS, shape memory substrates present unique alternatives to PDMS and other traditional elastomeric materials in the preparation of wrinkled surfaces. Often, a difference in deformation between the two layers is desirable to create a wrinkling effect. The shape memory effect allows a strain to be maintained in the absence of an external force, and wrinkle formation can be externally triggered by an external stimulus, such as temperature. There have been several examples of gold-sputtered shape memory elastomers for the preparation of wrinkled surfaces.[7,14,21] Mather *et al.* prepared a wrinkled bilayer system from a butyl acrylate copolymer and 33 nm of

gold and correlated the prestrain of the material with the wavelength and amplitude of the wrinkles.[14] Xie *et al.* also observed wrinkles on epoxy-based shape memory elastomers with a thin layer gold and utilized these materials to encode strain history.[7]

Herein, we describe the synthesis of a shape memory substrate that has been grafted with high-density polymer brushes and explore the wrinkling behavior of the materials. The shape memory elastomer used in this work, poly(octylene diazoadipate-*co*-octylene adipate), was originally reported by our group in previous work,[22] but has been modified to contain 13 mol% diethyl 2,5-diazidoadipate, the azide containing monomer, to achieve a T_m of 42 °C. The premise for this work is that grafting a polymer brush from the extended, temporary state should produce a higher density polymer brush upon return to the primary state than a brush grafted directly from the primary state due to the increased surface area and number of initiation sites available in the temporary shape. Given its tethered nature, this polymer brush behaves as an incompressible thin film on the surface of the strained shape memory substrate, resulting in mechanical instabilities that manifest as wrinkles.[19] To our knowledge, this is the first example of a covalently bound polymer brush layer being used to induce wrinkling on a shape memory substrate, and one of the few studies of wrinkling in elastomer-brush bilayer systems.

1.2 Experimental Methods

1.2.1 Materials

All materials were purchased from Sigma Aldrich, Fisher Scientific or VWR international and used as received unless otherwise noted. Oligio(ethylene glycol)

methacrylate ($OEGMA_{500}$) was purchased from Sigma Aldrich and passed over an alumina column prior to use.

1.2.2 Monomer and Polymer Characterization

Monomer and azide prepolymers were characterized in $CDCl_3$ using a Bruker 400 AVANCE ^1H NMR, TA Instruments Q200 differential scanning calorimeter (DSC), Perkin Elmer Pyris 1 TGA (thermogravimetric analyzer) (TGA), and Waters gel permeation chromatography (GPC) system in THF relative to polystyrene standards. Poly(OEGMA) brushes in solution were characterized in D_2O using a Bruker 600 ^1H NMR and with GPC in THF relative to poly(methyl methacrylate) standards.

1.2.3 Film Characterization

Instrumentation. Surface analysis of all films was accomplished with a Kratos Axis Ultra DLD X-ray Photoelectron Spectrometer (XPS), attenuated total reflectance Fourier transform infrared spectroscopy (ATR-FTIR) using a Bruker ALPHA FT-IR spectrometer, and static water-in-air contact angles, which were measured with a KSV instrument and imaging using the sessile drop method (with at least 6 different spots on one film). All SEMs were taken on an FEI Quanta 200 Field Emission Gun Environmental Scanning Electron Microscope in high vacuum mode. The samples were sputtered with ~2.8 nm of gold prior to imaging.

Image analysis. SEM images were analyzed using ImageJ to determine the feature size and wavelength of wrinkles. Both feature size and wavelength were measured in vertical rows on SEM images of 250x magnification. At least 290 measurements were made on each image from the entire image.

1.2.4 Monomer and Prepolymer Synthesis

Synthesis of diethyl 2,5-diazidoadipate.[22] Diethyl *meso*-2,5-dibromoadipate (12.67 g, 35.2 mmol) and sodium azide (9.15 g, 141 mmol) were added to a 1:1 mixture of H_2O and CH_3CN (100 mL). The reaction was stirred at r.t. for 18 h. The product was extracted with ethyl ether, dried with $MgSO_4$, and solvent removed by rotary evaporation. The monomer was used without further purification. Yield 9.33 g (93%). ^{1}H NMR δ (ppm): 4.27 (q, *J* = 8 Hz, 4H), 3.91 (t, *J* = 4 Hz, 2H), 2.00 – 1.94 (m, 2H), 1.82 – 1.78 (m, 2H), and 1.32 (t, *J* = 8 Hz, 6H).

Synthesis of poly(octalene diazoadipate-co-octalene adipate) prepolymer. Poly(ODA-co-OA) was synthesized according to literature,[22] with an adjustment to azide monomer ratio incorporated into the polymer. An example polymerization is as follows: 1.133 g (0.13 eq, 3.960 mmol) diethyl 2,5-diazoadipate, 3.874 g (0.87 eq, 26.50 mmol) adipic acid, 5.006 g (1.11 eq, 34.21 mmol) 1,8-octanediol and 1.056 g (10 wt%) Novozym 435 were combined in a flask at 80°C under N_2. The pressure was reduced by 80 torr/h to 20 torr and held for 18 h. The pressure was further reduced to ~2 torr and held for 18-48 h. The polymer was dissolved in CH_2Cl_2 or $CHCl_3$, filtered to remove catalyst and precipitated into cold MeOH (-78 °C). The product was collected by filtration and dried *in vacuo* at 40 °C. Yield: 6.57 g, 66%. ^{1}H NMR δ (ppm): 4.18 (t, *J* = 6 Hz, 4H), 4.02 (t, *J* = 4 Hz, 18H), 3.91 (t, *J* = 4 Hz, 2H), 3.62 (t, *J* = 6 Hz, 4H), 2.30 (b, 18H), 1.93 – 1.91 (m, 1H), 1.79 – 1.76 (m, 1H), 1.64-1.58 (b, 44H), and 1.31 (b, 52H).

Endcapping of poly(octalene diazoadipate-co-octalene adipate) prepolymer with 2-isocyanatoethyl methacrylate. The prepolymers were endcapped according to literature.[22] Briefly, 6.57 g prepolymer (1 eq, 2.43 mmol), 0.83 g 2-isocyanatoethyl

methacrylate (2.2 eq, 5.35 mmol) and 0.05 g $Sn(Oct)_2$ (5 mol%, 0.12 mmol) were combined in dry CH_2Cl_2 (200 mL) and stirred at r.t. for 18 h. The solution was reduced by rotary evaporation and the polymers were precipitated from CH_2Cl_2 or $CHCl_3$ into cold MeOH (-78 °C). The product was collected by filtration, dried *in vacuo* at r.t. and stored at -4 °C. Yield: 6.24 g (95%). ^1H NMR δ (ppm): 6.11 (s), 5.58 (s), 4.94 (m), 4.20 (t, *J* = 6 Hz, 4H), 4.03 (t, *J* = 8 Hz, 18H), 3.91 (t, *J* = 4 Hz, 2H), 3.51 (q, *J* = 5.3 Hz, 1H), 2.31 (t, 18H), 1.94 (s, 3H), 1.99 – 1.94 (m, 2H), 1.85 – 1.78 (m, 2H), 1.67-1.58 (b, 44H), and 1.32 (b, 52H).

1.2.5 Film Formation via Crosslinking

Poly(octalene diazoadipate-co-octalene adipate) methacrylate (1 g) and 2,2'-diethoxyacetophenone (3 drops) was dissolved in $CHCl_3$ (1-1.5 g). The solution was poured into a teflon mold and covered with a clean glass slide. The sample was irradiated with 365 nm UV light for 9.9 min. The sample was dried *in vacuo* at 60 °C for 24 h. The side of the sample facing the glass slide was used for ATR-FTIR, XPS, contact angle and SEM analysis after subsequent reactions.

1.2.6 Shape Programming and "Click" of ATRP Initiator

To program the substrate into a secondary shape, a 1-cm^2 crosslinked azide film was heated to 50 °C for 10 min, stretched 30% in a custom-made stretching device, and then cooled to -4 °C for 20 min. The film was removed from the stretching device and submersed in 10 ml EtOH in a closed vial under N_2. 1 ml of a $CuSO_4 \bullet 5H_2O$ solution (1 mg/ml), 1 ml of a sodium ascorbate solution (2.5 mg/ml) and 25 μL PBIB were added to the flask and stirred overnight. The film was washed briefly with agitation 3 x 20 mL water at room temperature, dried with forced air and then

overnight *in vacuo* at room temperature. The click reaction was monitored by the disappearance of the peak at 2100 cm^{-1} in ATR-FTIR.

Swelling analysis of click reaction. The initial weight and length of 7 azide substrates in their secondary shape were determined. Each sample was clicked overnight at room temperature, briefly rinsed with water and dried by dabbing with a lint-free paper towel before weight and length were determined. Gel fraction was determined by drying the samples at 80 °C *in vacuo* for 72 h and then weighing.

1.2.7 Kinetic Study of aqueous ARGET ATRP

Procedure is according to literature, with a few exceptions.[23] An ARGET ATRP catalyst stock solution was made from 4.46 mg $CuBr_2$, 66.1 mg TPMA, 1 ml H_2O and 0.75 mL DMF. An ARGET ATRP reaction solution was made from 15 mL $OEGMA_{500}$, 47.25 mL H_2O, 0.75 mL DMF, 0.86 mL ARGET ATRP catalyst stock solution, 300 mg NaCl and 129.5 mg PEGiBBr. An ascorbic acid solution was made from 56.5 mg ascorbic acid and 100 mL H_2O. All solutions stored at 4 °C until use. 8.5 mL of the ARGET reaction solution and a clicked substrate of ~1 cm^2 were purged with Ar for 30 min. To initiate the reaction, the ascorbic acid solution was continuously added to the flask via syringe pump at a rate of 4 μL min^{-1} for the desired amount of time at 25-26 °C. Aliquots were removed under Ar at indicated time points to perform ^1H NMR (D_2O) and GPC (THF) analysis.

1.2.8 Grafting-from Shape Memory Surfaces

To graft from a clicked surface, 8.5 mL of the ARGET reaction solution (omitting PEGiBBr) and a clicked substrate of ~1 cm^2 were purged with Ar for 30 min. To initiate the reaction, the ascorbic acid solution was continuously added to the flask

via syringe pump at a rate of 4 μL min^{-1} for the desired amount of time at 25–26 °C. To terminate reaction, the addition of ascorbic acid was stopped, the flask was opened and the substrate was removed and washed 3 x 20 mL with H_2O. The substrate was dried with forced air and then overnight *in vacuo* at room temperature. To return the substrates to their primary shape, they were heated to 70 °C for 10 min and then cooled to –4 °C for 20 min. Scheme 2.1 illustrates the complete shape memory grafting fabrication.

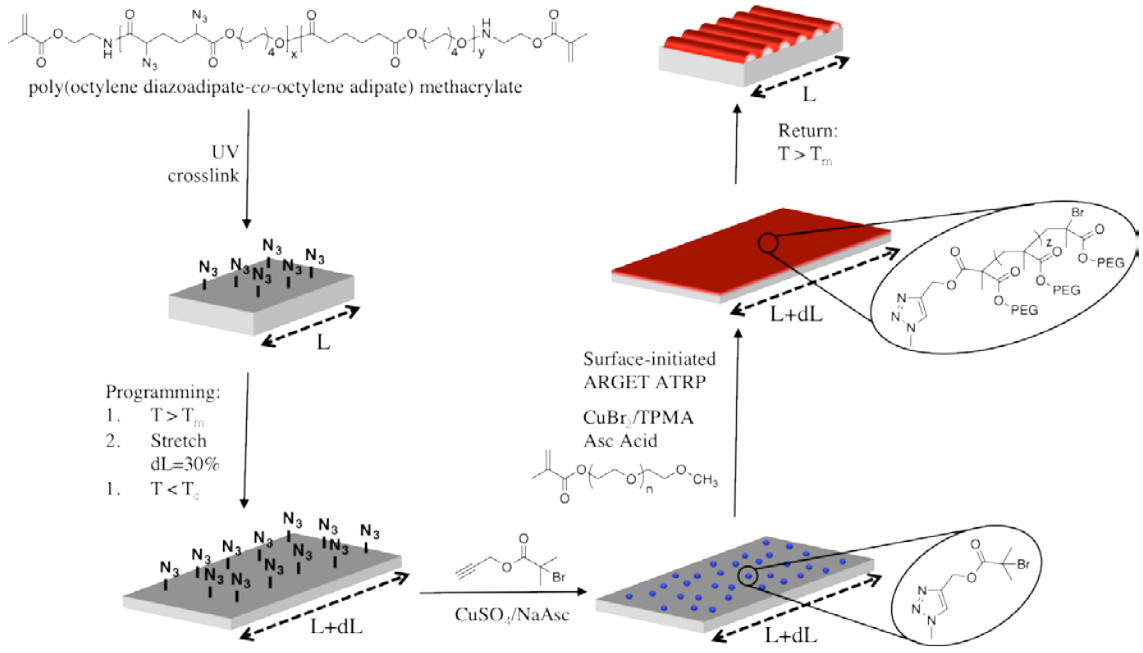

Scheme 1.1: Schematic for the fabrication of wrinkled substrates utilizing an azide-functionalized shape memory elastomer and poly(OEGMA) brushes.

Variation of equilibration time (t_1). A single clicked substrate in the secondary shape was cut into equal sections parallel to the direction of strain. These substrates were sequentially added to the ARGET reaction solution prior to addition of ascorbic acid at the indicated time points. When the last substrate was added to the solution, it was purged for 30 min with Ar prior to initiation by the addition of

ascorbic acid, and allowed to react for 6 h. Each sample was cut in half again, so that one end remained in the secondary shape, and the other was returned to the primary shape.

Variation of reaction time (t_2). A single clicked substrate in the secondary shape was cut into equal sections parallel to the direction of strain. These substrates were all added to the reaction solution and purged for 30 min with Ar prior to initiation with the addition of ascorbic acid. The reaction was allowed to proceed for 2h, at which point one substrate was removed. The reaction was resealed, purged with Ar for 20 min and then initiated by the addition of ascorbic acid. This was repeated for 4 and 6 h samples. Each sample was cut in half again, so that one end remained in the secondary shape, and the other was returned to the primary shape.

Swelling analysis of ARGET reaction solution. The initial weight and length of 6 clicked substrates in their secondary shapes were determined. Each sample was allowed to swell in ARGET solution at 25 °C for the indicated amount of time, removed from solution, rinsed briefly with water, dried by dabbing with a lint-free paper towel and then weighed and measured. The samples were returned to solution for additional time points.

1.3 Results and Discussion

1.3.1 Shape Memory Substrates

Poly(octylene diazoadipate-*co*-octylene adipate), shown in Scheme 1.1, was selected as the shape memory substrate because of the ability to post-functionalize

the surface after crosslinking into the primary shape. Brosnan *et al.* originally reported a polymer using 17 mol% of the diazidoadipate monomer which resulted in a T_m of 38 °C. To avoid a shape change and reduce swelling during synthesis of the polymer brushes, a higher transition temperature was desired, so the T_m was tuned to 42 °C by reducing the diazidoadipate monomer content to 13 mol%.

The click reaction was monitored by ATR-FTIR and XPS. In Figure 2.1a, ATR-FTIR shows the disappearance of the peak at 2100 cm^{-1}, which is indicative of the azide functionality. The XPS N1s spectrum, Figure 2.1b, shows a disappearance of the peak at 405 eV, which indicates the presence of the azide functionality, and also the appearance of a peak at 69 eV in the Br 3d spectrum (Figure 2.1c), indicating the presence of bromine.

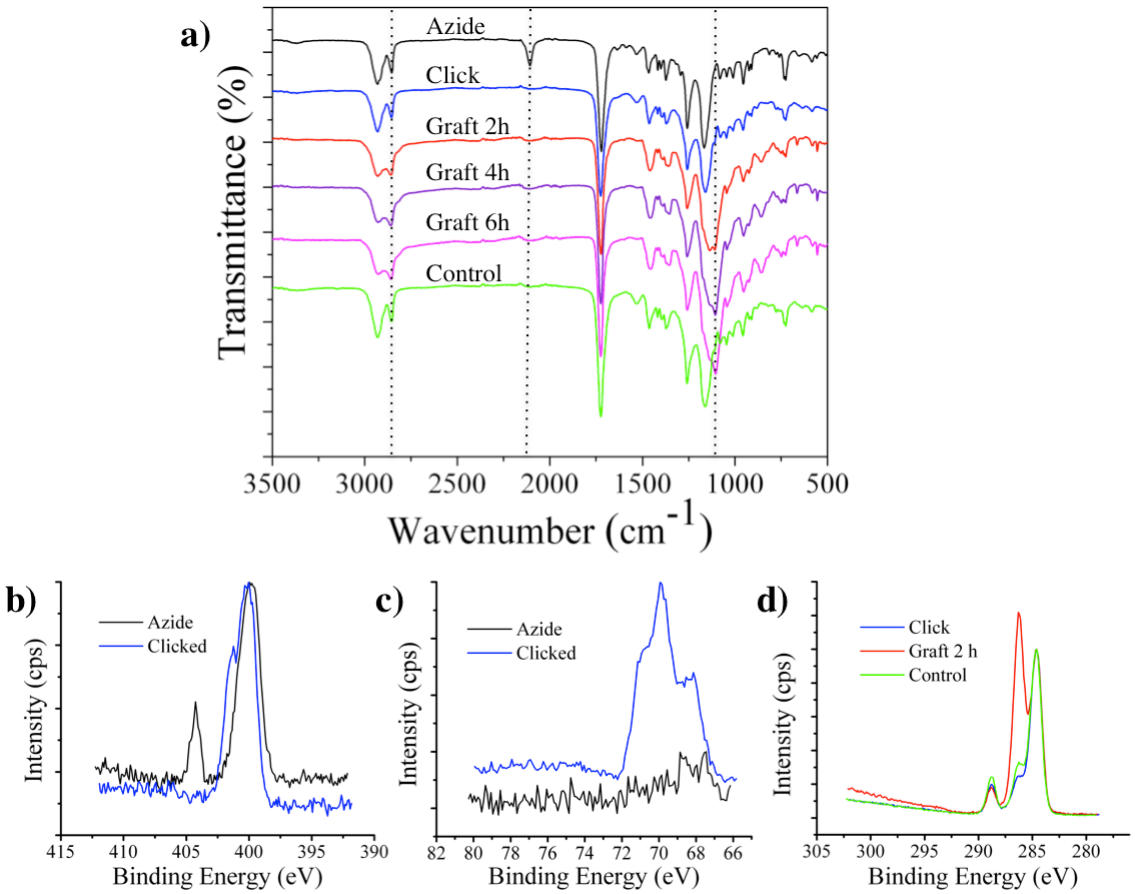

Figure 1.1: ATR-FTIR (a) and N 1s (b), Br 3d (c) and C 1s (d) XPS of azide, clicked, grafted and control substrates. Control substrates were immersed in the ARGET reaction solution at 25 °C in the absence of polymerization for 6 h.

1.3.2 "Grafting-from" via Aqueous ARGET ATRP

Using water as a solvent to produce polymer brushes was desired to inhibit swelling of the azide-functional elastomer substate. Aqueous ARGET (activators regenerated by electron transfer) ATRP of oligo(ethylene glycol) methacrylate, as reported by Simakova *et al.*,[23] was selected due to the ease of molecular weight control in water via the continuous addition of ascorbic acid. Additionally, the temperature of reaction was adjusted to 25 °C to prevent triggering the shape memory transition during the grafting reaction.

Using a sacrificial initiator, we have shown that in the presence of the clicked substrates there is a linear increase in molecular weight of polymer chains with time and addition of ascorbic acid, indicating that there are no termination, chain transfer, or initiation problems due to the presence of the substrates (Figure 2.2). For the remainder of the experiments, the polymer brushes were grown in the absence of a sacrificial initiator to prevent the adsorption of unattached growing chains to the surface.

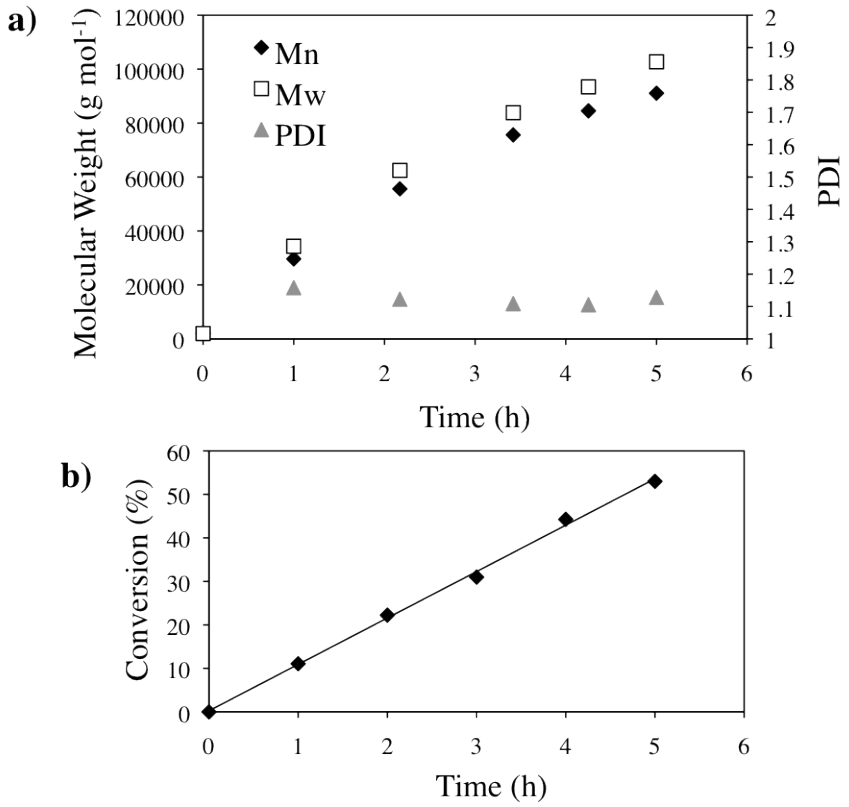

Figure 1.2: Molecular weight (a) and conversion (b) of polymers in solution in the presence of the clicked substrates.

The appearance of the poly(OEGMA) brushes was monitored by the appearance of C-O single bonds in ATR-FTIR and XPS. In the ATR-FTIR (Figure

1.1a), the appearance of peaks at 1100 cm^{-1}, attributed to the C–O–C asymmetric stretching absorption, and 2850 cm^{-1}, attributed to the C–O–C vibration absorption, indicate the increased presence of C–O bonds in comparison to the clicked substrate. In the XPS C1s spectrum, Figure 1.1d, the grafted substrates show the appearance of a peak at 287 eV, which indicates the presence of C–O single bonds.

A control sample was prepared by the submersion of a clicked sample in the ARGET reaction solution for 6h in the absence of ascorbic acid so that no polymerization occurred. The control sample looked identical to the clicked sample in both the ATR–FTIR and the XPS spectra, which indicates that the evidence for C–O single bond formation on the grafted samples in the ATR–FTIR and XPS is due to surface–initiated polymerization and not adsorption of OEGMA monomers.

In Figure 1.3, static water contact angle was used to further confirm the attachment of the polymer brushes, and also showed that surface properties can be varied with reaction time. With increased reaction time from 0–6 hrs, the contact angle decreased from 75° to 30°, which is lower than the reported contact angles of 40–52° for poly(OEGMA) surfaces in the literature,[24] possibly due to an increase in roughness due to surface morphology that will be discussed later. Control samples were prepared by submersing the clicked substrates in the ARGET solution in the absence of polymerization for the indicated amount of time. The contact angle for the control samples remained similar to that of the clicked substrate, indicating that the reduction in contact angle is not due to swelling or absorption, but is due to the presence of poly(OEGMA) brushes on the surface.

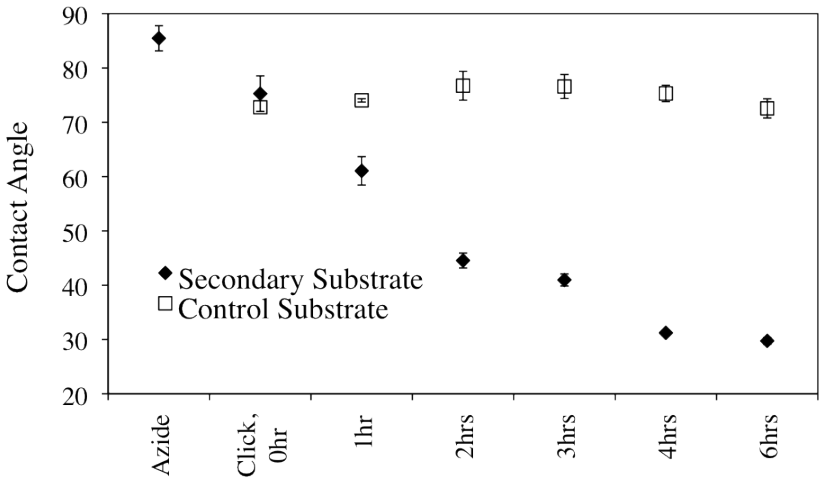

Figure 1.3: Static water contact angle for azide, clicked, grafted and control substrates in the secondary shapes. Control substrates were immersed in the ARGET reaction solution at 25 °C in the absence of polymerization for the indicated amount of time.

1.3.3 Surface Morphology and Wrinkling Behavior

Upon the grafting of poly(OEGMA) from the surface of a secondary substrate, we observed the presence of micron-sized, biaxial features by SEM. To return the grafted substrates to the primary shape, the materials were heated to 70 °C for 10 min, and cooled to ~4 °C for 10 min. Uniaxial wrinkles were observed on the returned substrates in addition to the features on the secondary substrate.

In an effort to understand the formation of the features and wrinkles, equilibration time (t_1) and reaction time (t_2) were investigated. Equilibration time is defined as the amount of time that the substrates were allowed to presoak in the ARGET ATRP solution prior to initiation of polymerization. Reaction time is the amount of time the ARGET ATRP reaction was allowed to progress before termination of the reaction by removal of the substrate from the ARGET solution.

In the SEM images in Figure 1.4, reaction time has been kept constant at 6h while equilibration time (t_1) has been varied from 0.5-21 h. The sample with the

minimum equilibration time, t_1=0.5 h, showed features on the secondary substrate as well as wrinkle formation on the returned substrate. For t_2 > 0.5 h, no feature or wrinkle formation was observed on the secondary or returned substrates.

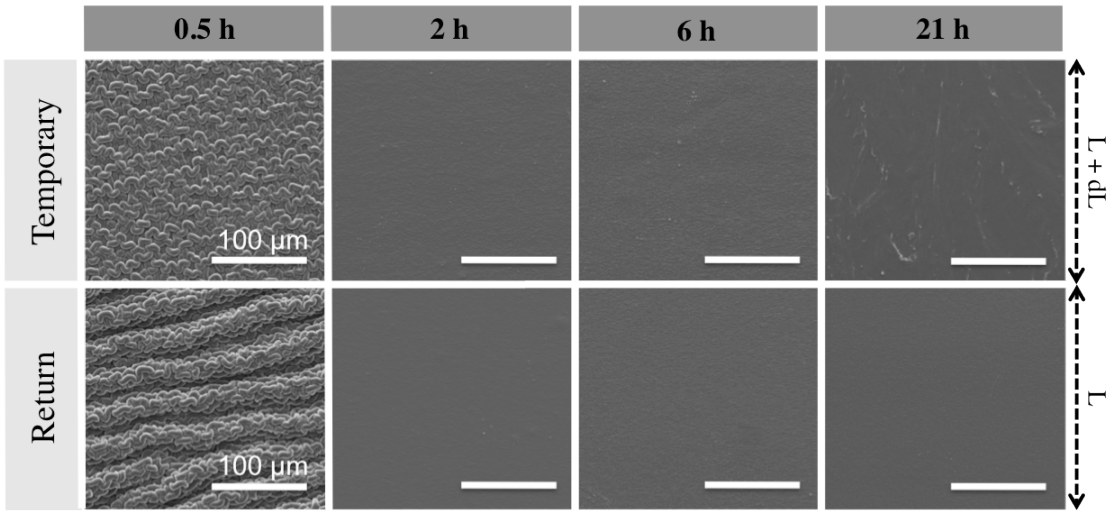

Figure 1.4: SEMs of grafted substrates varying equilibration time, t_1. The substrates were equilibrated in the ARGET reaction solution at 25 °C for 0.5, 2, 6 and 21 h prior to grafting of poly(OEGMA) for 6 h.

The pattern of the random surface morphology on the temporary shape indicates the wrinkling effect is most likely due to swelling of the surface. The observation that increased equilibration time in the reaction medium, t_1 (Figure 1.5), actually causes the disappearance of the random wrinkles seemingly opposes the observation of other swelling-induced wrinkling systems, where the internal osmotic pressure promotes wrinkling instabilities.[25] This finding prompted investigations into the swelling of the substrate during the click reaction and in the ARGET reaction solution. It was determined that the azide substrate increased 4.6 ± 0.6 wt% in the click reaction solution, but swelling in the ARGET solution was considerably less, reaching a maximum value of 2.4 wt% after 18 h (Figure 1.5). This

indicates that the substrates actually deswell in the ARGET reaction solution, so that with increased t_1, the internal osmotic pressure decreases. For t_1>0.5 h, the internal osmotic pressure has decreased below the critical value for wrinkling, so no wrinkles are observed.

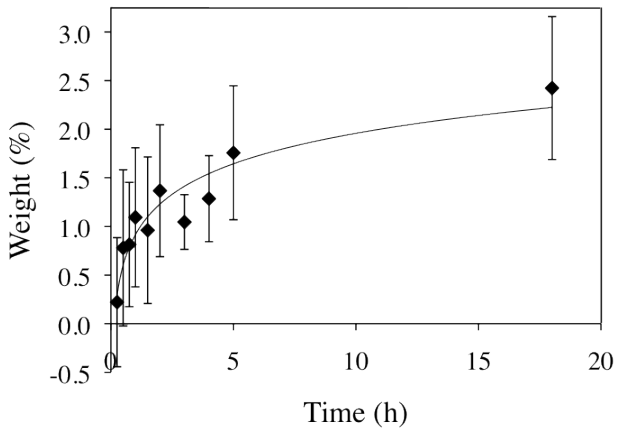

Figure 1.5 Swelling of the clicked substrates in the ARGET reaction solution at 25 °C.

In Figure 1.6, equilibrium time has been kept constant at 0.5 h, while reaction time has been varied for 0–6 h. As expected, there were no features or wrinkles formed on the secondary substrate for t_2 = 0 h because no brushes are present. This indicates that the presence of polymer brushes is necessary for the formation of features on the temporary substrate and wrinkles on the returned substrate. Interestingly, the t_2=2 h sample showed no feature formation on the temporary substrate, but wrinkles were observed on the returned substrate. This indicates that formation of uniaxial wrinkles on the return substrate is independent of the randomly oriented features on the temporary substrate, and that two mechanisms to induce wrinkling are present. It is likely that the critical osmotic pressure (P_c = 2/3 $(E_sE_f)^{1/2}$) to create swelling-induced features on the temporary shape has not

been reached, but the critical buckling strain (ε_c= ¼ $(3E_s/E_f)^{2/3}$) due to the deformation of the substrate to induce the formation of uniaxial wrinkles has been surpassed.[25,26,27] In the t_2=4 and 6 h samples, both the critical osmotic pressure and the critical buckling strain have been achieved, so both features and wrinkles are observed.

Feature size and wrinkle wavelength were investigated by analyzing the SEM images in Figure 1.6a, the result of which are in Figures 1.6b and c. By measuring the cross-sectional profile of the temporary substrate, we determined the average feature size to be 4.8 and 6.2 μm for the 4 and 6 h substrates, respectively. The size distribution for the 6 h substrate was much broader than for the 4 h substrate, which could be due to a lack of homogeneity of the substrate morphology of the clicked substrate, causing a larger variation of brush molecular weights, and thus a larger variety of feature sizes. The wavelengths of the 2, 4 and 6 h samples were 27, 30 and 33 μm, respectively, with larger size distributions for the samples with features on the temporary shape.

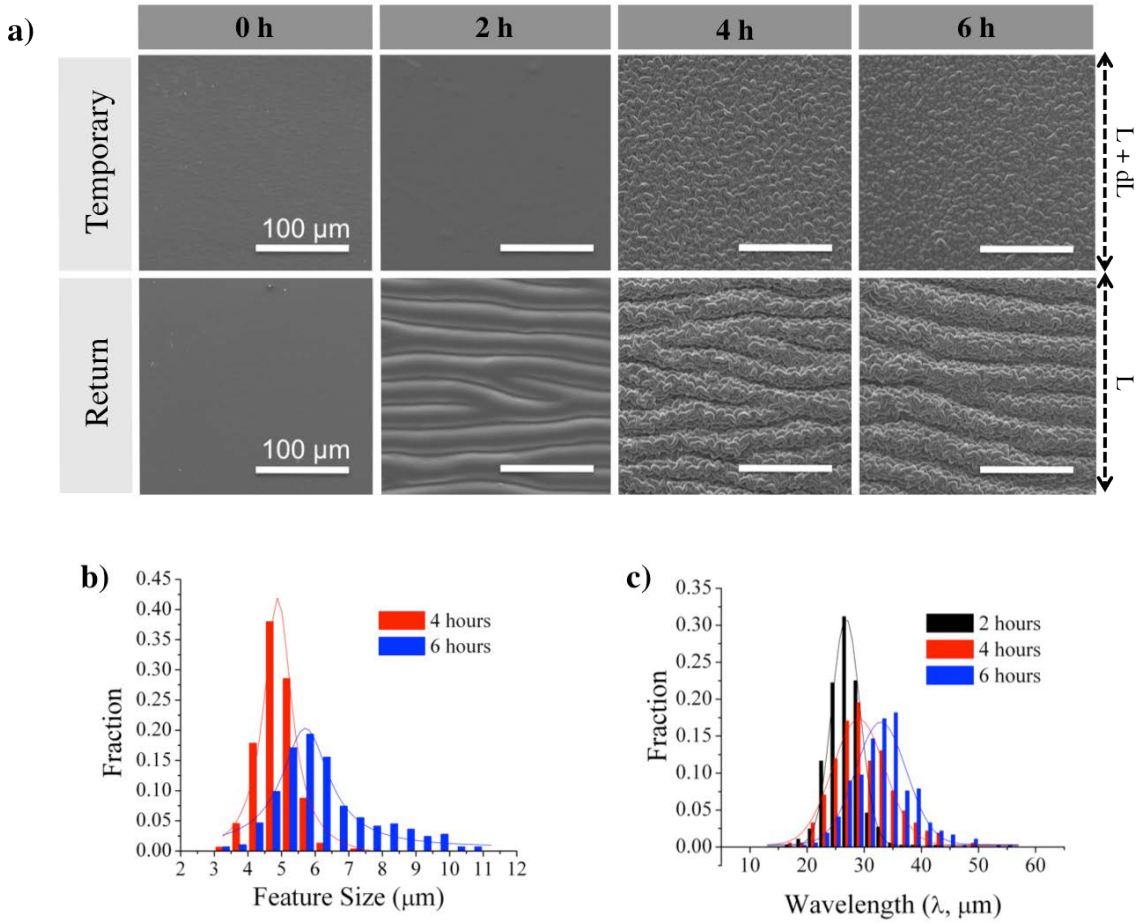

Figure 1.6 a) SEMs of ungrafted and grafted substrates varying reaction time, t_2. The substrates were equilibrated in the ARGET reaction solution at 25 °C for 0.5 h prior to grafting of poly(OEGMA) for 0, 2, 4 and 6 h. b) Feature size determination for the secondary substrates by image analysis. Average feature sizes were 4.9 ± 0.5 and 6.2 ± 1.4 μm for the 4 and 6 h substrates, respectively. c) Wavelength determination for the returned substrates by image analysis. Average wavelengths were 27 ± 3, 30 ± 5 and 33 ± 5 μm for the 2, 4 and 6 h substrates, respectively.

Classical wrinkling mechanics dictate that the wavelength, λ, of a wrinkled material, defined as[28]

$$\lambda = 2\pi h_f \left(\frac{\bar{E}_f}{3\bar{E}_s} \right)^{1/3}$$

is dependant on height of the top film, h_f, where E_f and E_s are the plane-strain moduli of the film and substrate, respectively. It can be assumed that h_f has a

positive correlation with reaction time, although it cannot be assumed that the relationship is linear. When comparing the wavelengths of the 2, 4 and 6 h samples, the larger wavelength of the 6 h sample is presumably due to a thicker brush layer. Alternatively, the 6 h sample also has a larger distribution than the 2 and 4 h substrates, so the larger wavelength could also be a function of the large size distribution observed for the feature sizes on the secondary substrate.

The wrinkles on the return substrate are due to a difference in strain between the shape memory substrate and the grafted brush layer. The high-density brushes grafted on the secondary shape are in an unstrained equilibrium conformation, while the substrate is in a strained secondary conformation. By triggering the return of the primary shape, the brush layer is unable to compress, leading to mechanical instabilities at the brush-substrate interface.

1.4 Conclusions

Poly(OEGMA) has been successfully grafted from a thermally-triggered shape memory elastomer, as confirmed by ATR-FTIR, XPS and static water contact angle. Upon grafting of the poly(OEGMA) brushes, swelling-induced biaxial features were observed, and upon return of the shape memory substrate to the equilibrium shape, uniaxial wrinkles were observed in addition to the biaxial features. Wrinkle and feature formation were determined to be a function of equilibration time, t_1, in the ARGET reaction solution due to swelling of the substrate. Wrinkle wavelength is positively correlated with reaction time, t_2, but additional experiments are needed to determine the dependence of the relationship. This is the first example of utilizing

grafted brushes to induce wrinkling on the surface of a shape memory polymer, and the combination of the two modes of wrinkling increases the complexity of the observed surface microstructures.

REFERENCES

(1) Genzer, J.; Groenewold, J. *Soft Matter* **2006**, *2*, 310–323.

(2) Li, B.; Cao, Y.-P.; Feng, X.-Q.; Gao, H. *Soft Matter* **2012**, *8*, 5728–5745.

(3) Yang, Shu.; Khare, K.; Lin, P.-C. *Adv. Func. Mater.* **2010**, *20*, 2550–2564.

(4) Lin, P.-C.; Yang, S. *Soft Matter* **2009**, *5*, 1011–1018.

(5) Lin, P.-C.; Vajpayee, S.; Jagota, A.; Hui, C.-Y.; Yang, S. *Soft Matter* **2008**, *4*, 1830–1835.

(6) Jeong, H. E.; Kwak, M. K.; Suh, K. Y. *Langmuir* **2010**, *26*, 2223–2226.

(7) Xie, T.; Xiao, X.; Li, J.; Wang, R. *Adv. Mater.* **2010**, *22*, 4390–4394.

(8) Kim, J. B.; Kim, P.; Pégard, N. C.; Oh, S. J.; Kagan, C. R.; Fleischer, J. W.; Stone, H. A.; Loo, Y.-L. *Nature Phototon.* **2012**, *6*, 327–332.

(9) Efimenko, K.; Findlay, J.; Callow, M. E.; Callow, J. A.; Genzer, J. *ACS Appl. Mater. Interfaces* **2009**, *1*, 1031–1040.

(10) Efimenko, K.; Rackaitis, M.; Manias, E.; Vaziri, A.; Mahadevan, L.; Genzer, J. *Nature Mater.* **2005**, *4*, 293–297.

(11) Khang, D. Y.; Jiang, H. Q.; Huang, Y.; Rogers, J. A. *Science* **2006**, *311*, 208–212.

(12) Li, Z.; Zhang, S.; Zhang, P.; Yang, D.; Jin, G.; Ma, H. *Polym. Adv. Technol.* **2012**, *23*, 1240–1245.

(13) Bowden, N.; Brittain, S.; Evans, A. G.; Hutchinson, J. W.; Whitesides, G. M. *Nature* **1998**, *393*, 146–149.

(14) Yang, P.; Baker, R. M.; Henderson, J. H.; Mather, P. T. *Soft Matter* **2013**, *9*, 4705–4714.

(15) Chan, E. P.; Smith, E. J.; Hayward, R. C.; Crosby, A. J. *Adv. Mater.* **2008**, *20*, 711–716.

(16) Alzahrani, A. A.; Nair, D. P.; Smits, D. J.; Saed, M.; Yakacki, C. M.; Bowman, C. N. *Chem. Mater.* **2014**, *26,* 5303–5309.

(17) Chung, J. Y.; Chastek, T. Q.; Fasolka, M. J.; Ro, H. W.; Stafford, C. M. *ACS Nano* **2009**, *3*, 844–852.

(18) Huang, H.; Chung, J. Y.; Nolte, A. J.; Stafford, C. M. *Chem. Mater.* **2007**, *19*, 6555–6560.

(19) Milner, S. T. Polymer Brushes. *Science* **1991**, *251*, 905–914.

(20) Barbey, R.; Lavanant, L.; Paripovic, D.; Schüwer, N.; Sugnaux, C.; Tugulu, S.; Klock, H.-A. *Chem Rev.* **2009**, *109*, 5437–5527.

(21) Fu, C.-C.; Grimes, A.; Long, M.; Ferri, C. G. L.; Rich, B. D.; Ghosh, S.; Ghosh, S.; Lee, L. P.; Gopinathan, A.; Khine, M. *Adv. Mater.* **2009**, *21*, 4472–4476.

(22) Brosnan, S. M.; Brown, A. H.; Ashby, V. S. *J. Am. Chem. Soc.* **2013**, *135*, 3067–3072.

(23) Simakova, A.; Averick, S. E.; Konkolewicz, D.; Matyjaszewski, K. *Macromolecules* **2012**, *45*, 6371–6379.

(24) Fan, X.; Lin, L.; Messersmith, P. *Biomacromolecules* **2006**, *7*, 2443–2448.

(25) Tanaka, T.; Sun, S. T.; Hirokawa, Y.; Katayama, S.; Kucera, J.; Hirose, Y.; Amira, T. *Nature* **1987**, *325*, 796–798.

(26) Guvendiren, M.; Yang, S.; Burdick, J. A. *Adv. Func. Mater.* **2009**, *19,* 3038–3045.

(27) Huang, Z. Y.; Hong, W.; Suo, Z. *J. Mech. Phys. Solids* **2005**, *53*, 2101–2118.

(28) Huang, R. *J. Mech. Phys. Solids* **2005**, *53*, 63–89.

Chapter II
SOLUTION AND HETEROGENOUS POLYMERIZATION OF IODINE-CONTAINING METHACRYLATE COPOLYMERS FOR BIOMATERIAL APPLICATIONS

2.1 Introduction

Some of the most common major orthopedic surgical procedures performed annually are hip replacements, knee replacements, balloon kyphoplasty and vertebroplasty, and with the aging population growing, the instances of these surgeries is expected to rise.[1,2,3] Injectable acrylic bone cements, most often composed of poly(methyl methacrylate) (PMMA), are a vital component to these procedures.[4] In joint replacement surgeries, bone cement is used to immobilize the prosthesis in the bone and to transfer body weight from the prosthesis to the bone. In vertebroplasty and balloon kyphoplasty, the cement is injected into a fractured vertebral body to stabilize and restore height. Commercial bone cements are comprised of a powder and a liquid portion that are mixed together immediately prior to injection. The powder contains PMMA beads, an inorganic radiopacifier and an initiator, benzoyl peroxide (BPO). The liquid contains methyl methacrylate (MMA) monomer and an accelerator, *N, N*-dimethyl-*p*-toluidine (DMPT).[2,5]

For all applications, X-ray visibility is necessary to monitor cement injection, prosthesis placement and changes in the cement over time. To achieve radiopacity, inorganic fillers, such as $BaSO_4$ and ZrO_2, are mixed into the cement. For the fixation of artificial joints, the powder portion contains 8-15 wt% $BaSO_4$ or ZrO_2.[5,6] Higher

proportions of filler are needed for vertebral fracture repair because the surgery is guided by fluoroscopic X-ray.[7] While inorganic additives make the cements easier to visualize by X-ray, there are some major mechanical and biological drawbacks.

Mechanically, the presence of these fillers can compromise the tensile strength[8,9] and fracture toughness[10] of the cements and promote crack propagation.[11] Poor adhesion between the inorganic phase with the polymeric matrix, inefficient transfer of stress from the matrix to the fillers and aggregation of inorganic particles are to blame for the shortcomings of these composites.[12,13,14] Fractures in the cement reduce implant lifetime, causing damage to surrounding tissue and necessitating the need for additional surgery to reattach the prosthesis or refill the vertebral cavity. Biologically, the presence of the inorganic additives can trigger macrophague-osteoclast differentiation that contributes to bone resorption and aseptic loosening.[15] Additionally, the radiopacifier particles can become dislodged from the cement and enter the joint space, causing damage to the surfaces and increase the production of polyethylene wear debris.[16,17,18]

To address the issues associated with the addition of inorganic fillers, new iodine-containing polymerizable monomers have been developed for the synthesis of new bone cement materials.[19,20,21,22] These monomers can provide X-ray contrast to radiolucent PMMA materials by either incorporating them into the liquid or the solid portion of the bone cement, thus eliminating the need for the addition of $BaSO_4$ and ZrO_2. These materials have showed great promise in providing sufficient contrast while maintaining the desired mechanical behavior. All of the monomers

developed to date are aromatic based monomers with one to three iodines substituted on the aromatic ring.

Herein, we have developed a novel polymerizable monomer based on methyl methacrylate containing only aliphatic-bound iodine. The advantage of this monomer over previously synthesized iodine monomers is the high weight percent of iodine present in the monomer, which enables the incorporation of fewer functionalized monomers to obtain the desired radiopacity while also limiting the effect on mechanical properties. The iodine on this monomer is resistant to elimination and displacement due to the unique structure

2.2 Experimental Methods

2.2.1 Materials

Methyl methacrylate (99%) was de-inhibited with adsorption alumina. Benzoyl peroxide (98%) was recrystallized from diethyl ether and methanol or precipitated from $CHCl_3$ with the addition of methanol. Methylene chloride was distilled from CaH_2. All other materials were used as received from Sigma Aldrich, Fisher Scientific or VWR international. All reactions performed under inert atmosphere (N_2) unless otherwise noted.

2.2.2 Monomer and Polymer Characterization

Monomer and copolymers were characterized in $CDCl_3$ using a Bruker 400 AVANCE ^1H NMR or a Bruker 600 ^1H NMR, TA Instruments Q200 differential scanning calorimeter (DSC), Perkin Elmer Pyris 1 TGA (thermogravimetric analyzer) (TGA),

and Waters gel permeation chromatography (GPC) system in THF relative to poly(methyl methacrylate) standards.

2.2.3 Microsphere Characterization

Scanning electron microscopy (SEM). All SEMs were taken on a FEI Quanta 200 Field Emission Gun Environmental Scanning Electron Microscope in high vacuum mode. The samples were sputtered with ~2 nm of gold prior to imaging. Images were analyzed with ImageJ software to measure the diameters of the beads and determine the PDI.

Electron dispersion spectroscopy (EDS). Iodine content was obtained by EDS using INCA PentaFet –x3 installed on an Hitachi S-4700 FESEM with an Si(Li) detector. Three areas of ~100 μm^2 were mapped and averaged to determine iodine content.

2.2.4 Bone Cement Characterization

X-ray computed tomography (CT). CT scans were performed on a GE eXplore speCZT CT 120 with an x-ray tube voltage of 70 kV, an x-ray tube current of 50 mA, and an exposure time of 32 ms. Resolution of the reconstructions is 100 μm. To determine the Houndsfiend units, the images of the samples from three different layers was averaged in ImageJ.

Compression Modulus. Compression modulus was determined on an Instron 4411 with a 5 kN load cell, a compressive rate of 0.5 mm/min, and data collection at 10 Hz. The samples were approximately 4.6 mm in diameter, and cut to a length that was twice the diameter. The slope of the linear portion was used to determine the modulus.

2.2.5 Preparation of Monomer

Preparation of 3-iodo-2,2-bis(iodomethyl)propanol. 3-Bromo-2,2-bis(bromomethyl)propanol (14.99 g, 46.2 mmol) was refluxed at 75 °C in saturated solution of sodium iodide (103.8 g, 692.5 mmol) in acetone (400 mL) for five days. The solution was filtered, and the solvent was removed by rotary evaporation. The yellow oil was redissolved in ethyl acetate and the organic layer was extracted with 5% sodium thiosulfate, water and brine and then dried over $MgSO_4$. The organic layer was filtered and then dried by rotary evaporation to a yellow oil, washed with hexanes and filtered to yield a white crystalline solid. Yield: 16.52 g (35.5 mmol, 76.8%) ^{1}H NMR (600 MHz, $CDCl_3$, δ): 3.72 (s, 2H, HO-C*H*$_2$), 3.36 (s, 6H, I-C*H*$_2$).

Preparation of 3-iodo-2,2-bis(iodomethyl)propyl methacrylate (IMMA). To a solution of *3*-iodo-2,2-bis(iodomethyl)propanol (16.52 g, 35.5 mmol) and triethylamine (7.5 mL, 53 mmol) in dry CH_2Cl_2 (200 mL), methacryloyl chloride (5.2 mL, 53 mmol) was added dropwise at 0°C. The solution was allowed to warm to room temperature and stir overnight. The solution was filtered and the organic layer washed with water (2x) and brine (1x) and then dried over $MgSO_4$. The solution was filtered and dried by rotary evaporation. The yellow oil was purified by column chromatography in ethyl acetate and hexanes (87.5:12.5, R_f=0.595) followed by recrystallization from hot hexanes (~400 mL). White, needle-like crystals were collected and washed with cold hexanes. Yield: 11.93 g (22.4 mmol, 63.0 %). ^{1}H NMR (600 MHz, $CDCl_3$, δ): 6.11 (s, 1H, *H*$_2$C=C), 5.63 (s, 1H, *H*$_2$C=C), 4.25 (s, 2H, O-C*H*$_2$), 3.39 (s, 6H, I-C*H*$_2$), 1.97 (s, 3H, C=C-C*H*$_3$).

2.2.6 Preparation of Microspheres by Solvent Evaporation

Solution polymerization of poly(MMA-IMMA) copolymers. An example reaction is as follows: A solution of AIBN in toluene was prepared (9.2 mg AIBN, 18.0 mL toluene). To 7.50 mL of the AIBN solution, add MMA (5.87 g, 58.5 mmol) and IMMA (2.98 g, 5.58 mmol). The solution was purged with Ar for 20 min at r.t. The reaction was heated to 70 °C and allowed to proceed for 20 h. The reaction cooled to rt, dissolved in CH_2Cl_2 and precipitated into MeOH. ^{1}H NMR (600 MHz, $CDCl_3$, δ): 4.04 (m, H_2C-O-), 3.60 (s, 3H, -C-CH_3), 3.39 (s, 6H, I-CH_2), 2.10-1.65 (m, 2H, H_2C-C), 1.29-0.51 (m, 3H, -C-CH_3).

Solvent evaporation of copolymers. . An example procedure is as follows: A polymer solution was prepared at a concentration of 0.075g/mL $CHCl_3$. In a beaker, 30 mL of the polymer solution was added to a solution of sodium dodecyl sulfate (SDS) (2 w/v%, 150 mL) while stirring at a rate of 500 rpm, and was allowed to stir at this rate while covered for 1 hr. The cover was removed and the solution was allowed to stir overnight. The microspheres were collected via filtration, washed with water and dried *in vacuo* at 30 °C overnight.

2.2.7 Suspension Polymerization of Copolymers

An example procedure is as follows: A 0.24% stabilizer solution was prepared from polyvinylpyrrolidone (Povidone-k) (0.5231 g PVP, 218 mL H_2O). 50 mL of the PVP solution was combined with 0.0785 g L-ascorbic acid and 2.525 g NaCl in a 100 mL 3-neck flask equipped with a rare-earth magnetic stir bar and a reflux condenser. The solution was stirred at a rate of 1050 rpm under N_2. MMA and IMMA (14.15 g total) were combined with BPO (0.25 mol%) and the clear solution was added to the PVP solution via needle. The solution was lowered into an oil bath at 70 °C and

allowed to proceed for 4 hrs. The reaction was terminated by filtering the beads and rinsing with H_2O (500 mL) and drying *in vacuo* at 30 °C overnight. ^1H NMR (600 MHz, $CDCl_3$, δ): 4.04 (m, H_2C-O-), 3.60 (s, 3H, -C-CH_3), 3.39 (s, 6H, I-CH_2), 2.10-1.65 (m, 2H, H_2C-C), 1.29-0.51 (m, 3H, -C-CH_3).

2.2.8 Preparation of Bone Cement

Bone cements were prepared from 60 wt% solid and 40 wt% liquid. The solid portion was comprised of 0.7375 g polymer beads (PMMA or copolymer) and 0.0125 g BPO. The liquid portion was comprised of 0.178 g DMPT and 8.714 g MMA. The solid portion (0.75 g) was mixed with 0.5 g of the liquid portion in a plastic dish in air. The cement was mixed for 45 seconds and then the resulting paste was put into a 1 mL syringe and compressed against the benchtop to create a cylinder. The cements were allowed to cure at room temperature. For the bone cement containing 10 wt% $BaSO_4$, $BaSO_4$ (0.0922 g), PMMA beads (0.6453 g) and BPO (0.0125 g) were mixed with 0.5 g of the liquid portion in the same manner as the other bone cements.

2.3 Results and Discussion

2.3.1 Iodinated Monomer Preparation

The methacrylate-functionalized iodine containing monomer, 3-iodo-2,2-bis(iodomethyl)propyl methacrylate (IMMA), synthesized in this work provides a high weight % iodine and is non-aromatic which can be co-polymerized with methyl methacrylate (Scheme 2.1). To our knowledge, all other iodinated monomers for bone cement applications utilize aromatically bound iodine to enhance the stability

of monomer, but this affords a lower weight % iodine and can alter the mechanical properties of the bone cement significantly.

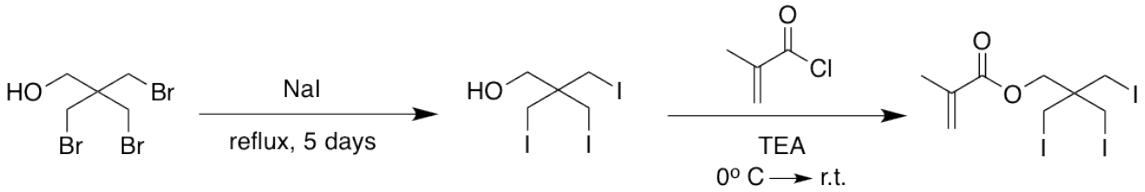

Scheme 2.1 Synthesis of IMMA monomer.

Most alkyl halides are good leaving groups and are therefore susceptible to elimination or substitution reactions and are therefore not suitable for *in vivo* applications. The primary structure of the iodine of IMMA makes E_1, S_N1 and radical reactions unfavorable. The lack of β-hydrogens makes E_2 reactions, unfavorable, but the iodine is still available for displacement by S_N2 with moderate to strong nucleophiles (Scheme 2.2).

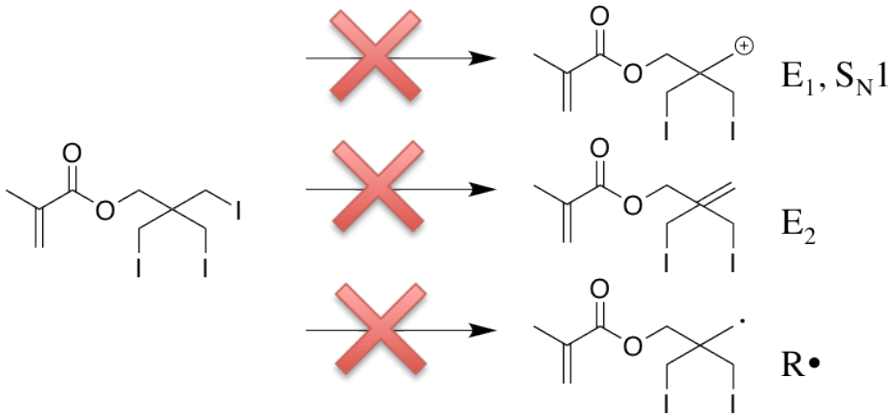

Scheme 2.2 The limited susceptibility of IMMA to E_1, S_N1, E_2 and radical reactions due to the primary structure of the iodine and the lack of β-hydrogens.

2.3.2 Solution Polymerization of Copolymers

Copolymerization of IMMA with MMA, as seen in Scheme 2.3, was first attempted in solution with a targeted molecular weight of approximately 400,000 g

mol^{-1}, as this was previously reported to be an ideal molecular weight for the powder portion of bone cement materials. Initially, polymers of three different feed ratios, f_{IMMA}=4.7, 9.1 and 16.7 mol%, were synthesized at 100 °C, and the resulting copolymer ratios were F_{IMMA}=7.8, 14.0 and 27.2 mol%. Suspecting that loss of MMA due to a low vapor pressure at the reaction temperature was the cause for the increased incorporation of the IMMA monomer into the polymer, the temperature of the reaction was lowered to 70 °C. At the lower reaction temperature f_{IMMA}=4.8, 8.7 and 14.0 mol%, and the resulting incorporation into the copolymer were F_{IMMA}=5.6, 10.3 and 17.5 mol%. Lowering the temperature reduced the loss of MMA, although the rate of incorporation of IMMA into the polymer was still higher than unity. This could be due to loss of MMA during reaction, or a reactivity difference between the two monomers (Figure 2.1).

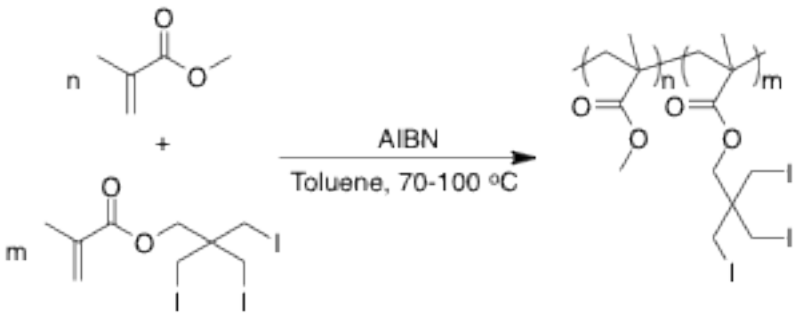

Scheme 2.3 Solution copolymerization of IMMA with MMA.

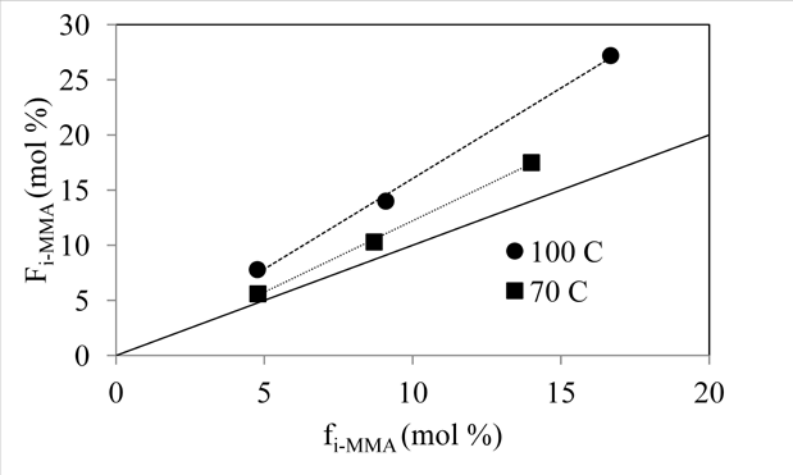

Figure 2.1 Polymer composition, F_{IMMA}, as a function of feed ratio, f_{IMMA}, of the IMMA monomer synthesized by solution polymerization.

Utilizing a reaction temperature of 70 °C, a variety of copolymer compositions were synthesized varying the feed ratio of 6.0–27.0 mol% IMMA resulting in polymers with 17.1–47.6 wt% iodine. The maximum feed ratio of IMMA is ~30 mol% due to the limited solubility of the IMMA in MMA and toluene. Table 3.1 includes the molecular weights of the copolymers synthesized.

Table 2.1 Compositions and Molecular Weights of Copolymers Synthesized in Toluene at 70 °C

Polymer	wt% Iodine	Molecular Weight (g mol^{-1}) $\langle M_n \rangle$	$\langle M_w \rangle$	PDI
P(MMA-*co*-IMMA$_{6.0}$)	17.1	430,000	632,000	1.50
P(MMA-*co*-IMMA$_{8.0}$)	22.3	360,000	540,000	1.50
P(MMA-*co*-IMMA$_{10.0}$)	27.1	451,000	706,000	1.49
P(MMA-*co*-IMMA$_{18.0}$)	37.9	405,000	632,000	1.56
P(MMA-*co*-IMMA$_{27.0}$)	47.6	371,000	589,000	1.59

The thermal degradation of the resulting copolymers is similar to that of a PMMA material prepared by similar methods. This indicates that the onset of degradation is not triggered by the elimination of the iodine moieties, but is due to the thermal degradation of poly(methyl methacrylate). The thermal stabilities of the copolymers reflect the stability of the iodine monomer and the unfavorable loss of iodine by elimination or radical pathways (Table 2.2).

Table 2.2 Thermal Degradation Temperatures of Polymers Prepared by Solvent Polymerization

Polymer	wt% Iodine	Degradation (°C)	
		5%	10%
PMMA	0.0	412	433
P(MMA-IMMA$_{6.0}$)	17.1	417	432
P(MMA-IMMA$_{8.0}$)	22.2	411	426
P(MMA-IMMA$_{10.0}$)	27.1	420	433
P(MMA-IMMA$_{14.0}$)	33.2	404	416
P(MMA-IMMA$_{18.0}$)	37.9	410	420

To determine if additional chain transfer was occurring due to the presence of the iodinated monomer, the iodinated alcohol, pentaerythritol triiodide (I-OH), was added to a polymerization of PMMA in bulk and in solution and compared to an identical reaction without the monomer. In this way, the iodinated moieties were introduced without influencing kinetic differences due to differences in reactivity between the two monomers. In the bulk reactions, the molecular weight and PDIs were identical, indicating that no chain transfer was occurring. In the solution reaction, a depression in molecular weight and PDI was observed. If chain transfer were occurring, we would expect to see a broadening of the PDI and a reduction in

molecular weight, so it can be concluded that the presence of the iodine monomer may be retarding the polymerization rate of MMA, but not causing chain transfer.

2.3.3 Fabrication of Microbeads by Solvent Evaporation

The synthesized copolymers were utilized to fabricate microbeads by a solvent evaporation method. In solvent evaporation, the polymer is dissolved in a good solvent, in this case chloroform, and a miniemulsion is formed upon addition to a continuous aqueous phase containing a stabilizer, in this case sodium dodecyl sulfate. The chloroform is then allowed to evaporate over several hours, resulting in a dispersion of microspheres. SEM images of PMMA and copolymer beads in Figure 2.2 show the spherical morphology attained utilizing this method.

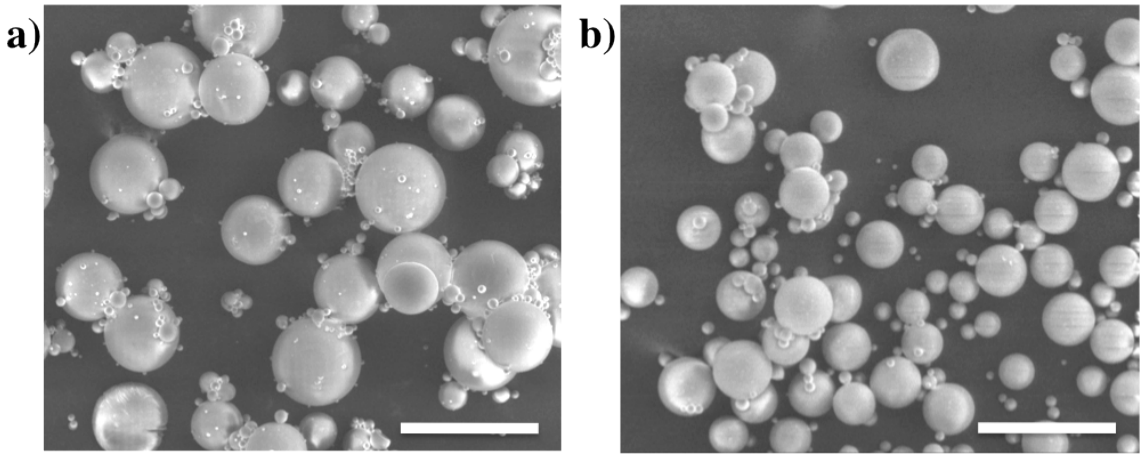

Figure 2.2 SEM images of microspheres fabricated with 2 wt% SDS solution by solvent evaporation. a) PMMA b) P(MMA-*co*-IMMA$_{6.0}$) . Scale bar=100 μm.

This method was first performed on PMMA beads by varying the concentration of SDS from 1-5 wt%. A 2 wt% solution of SDS yielded PMMA microspheres with diameters of 23 ± 14 μm. Solvent evaporation of the 17.1 wt% I copolymer yielded microspheres with similar diameters, 24 ± 11 μm (Table 2.3). A

large polydispersity is common with solvent evaporation methods, but is also common with other bone cement materials, so this would not present a challenge to the utilization of these materials in bone cement.

Table 2.3 Diameter of Microspheres Prepared by Solvent Evaporation

SDS wt%	Polymer	Diameter (μm)	PDI
1%	PMMA	18 ± 14	0.6
2%	PMMA	23 ± 14	0.39
3%	PMMA	22 ± 18	0.71
4%	PMMA	19 ± 13	0.48
5%	PMMA	19 ± 14	0.61
2%	P(MMA-*co*-IMMA$_{6.0}$)	24 ± 11	0.22

2.3.4 Suspension Polymerization of Copolymers

Following the initial successes utilizing solvent-based homogenous reaction conditions, a suspension polymerization method was implemented, as shown in Scheme 2.4. The vast majority of reports on bone cements utilize suspension polymerization because it enables the synthesis of beads in the ideal size and molecular weight range, while also being a one-step process. Representative images of copolymer and PMMA beads made by this method are in Figure 2.3. In this work, poly vinyl pyrrilidone (PVP) was utilized as a stabilizer with a stir speed of 1050 rpm and the variables of initiator concentration and stabilizer concentration were varied to tune the molecular weight and bead diameter, respectively.

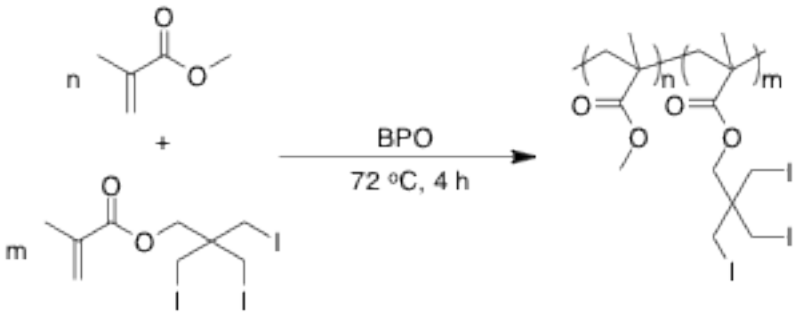

Scheme 2.4 Suspension polymerization of P(MMA-IMMA) copolymers.

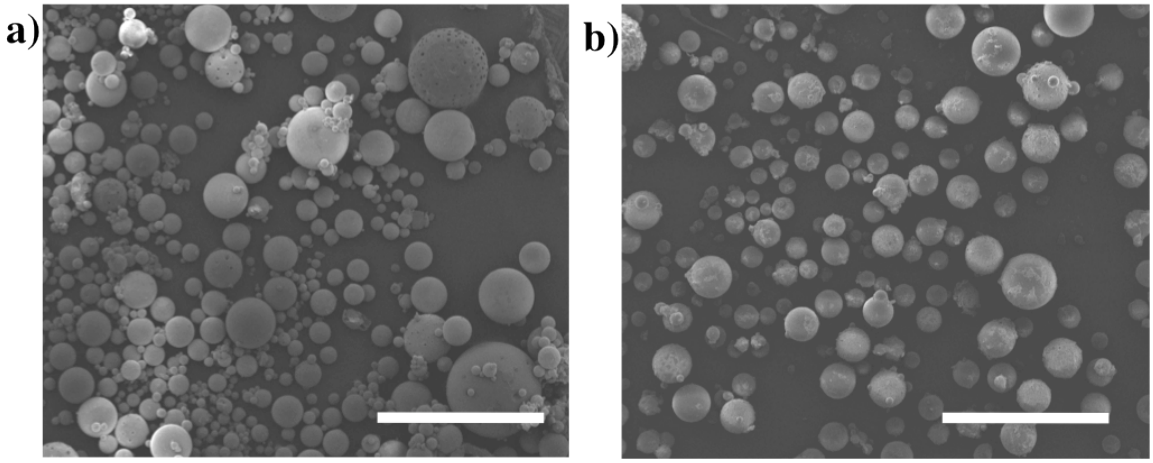

Figure 2.3 SEM images of microspheres fabricated with 0.24% PVP, and0.25% BPO by suspension polymerization. a) PMMA b) P(MMA-*co*-IMMA$_{6.9}$). Scale bar=100 μm.

2.3.4.1 Molecular Weight and Bead Diameter

Employing a suspension polymerization method with a feed ratio of f_{IMMA}=6.9 mol%, the molecular weight was tuned by varying the concentration of the initiator, BPO, from 0.02 to 0.15 mol% (Figure 2.4). The molecular weight generally increased in a linear fashion with decreasing initiator concentration, and experimental molecular weights were slightly higher than the target molecular weights. Targeting a M_W=360,000 g mol^{-1} and a feed ratio of f_{IMMA}=6.9 mol%, the bead diameter was tuned from 370-42 μm by changing the concentration of the stabilizer, PVP, from

0.15-0.25 wt% (Figure 2.5). As expected with suspension polymerization, the bead diameter decreased with increasing PVP concentration, with a minimum bead size ~40 μm.

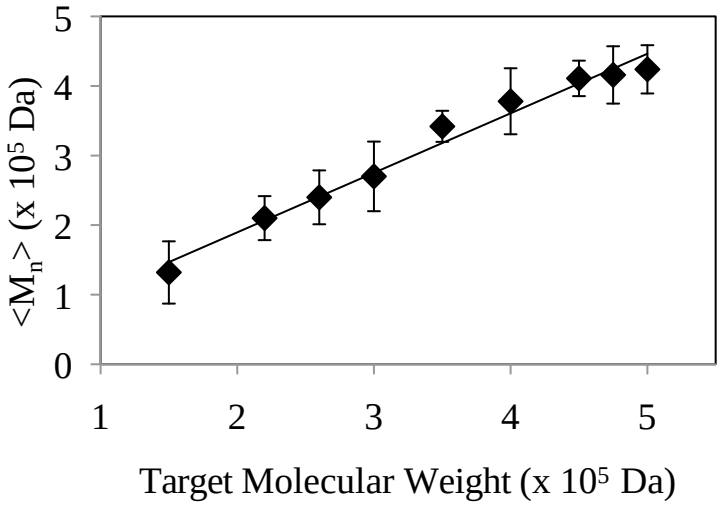

Figure 2.4 Experimental $<M_n>$ of the suspension polymerization of P(MMA-IMMA) copolymers. [BPO]=0.02 to 0.15 mol%.

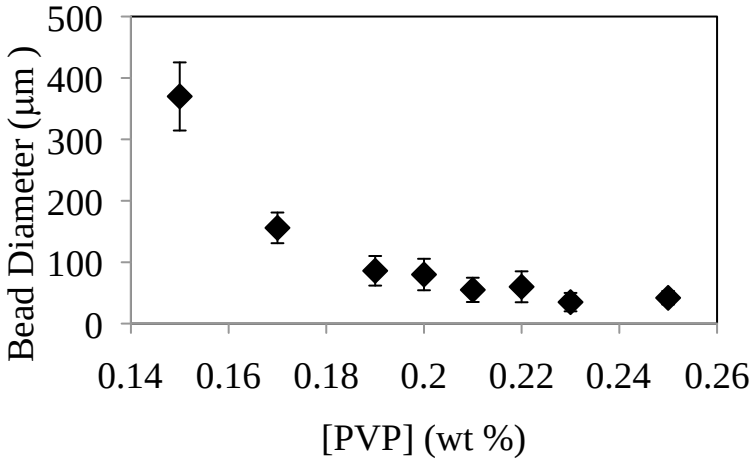

Figure 2.5 PVP concentration effect on bead diameter in the suspension polymerization of P(MMA-IMMA) copolymers with a feed ratio of f_{IMMA}=6.9 mol%.

The reaction was optimized to get beads with molecular weights of $<M_n>\sim 3.6 \times 10^5$ g mol^{-1} and bead size of ~50 μm by using a BPO concentration of

0.25% and a PVP concentration of 0.24%. Copolymers with a variety of compositions with the desired molecular weight and bead size were successfully synthesized. The results of which are in Table 2.4 and Table 2.5. Also, it should be noted that the copolymer composition has a lower content of the iodinated monomer than the feed ratio ($F_{IMMA}<f_{IMMA}$), which will be discussed in a later section. As expected, the thermal stabilities of the synthesized copolymer beads in Table 2.6 were similar to non-iodinated PMMA and the copolymers synthesized by solution polymerization (Table 2.2).

Table 2.4 Molecular Weight of PMMA and P(MMA-IMMA) Copolymer Beads by Suspension Polymerization

Polymer	$f_{I\text{-}MMA}$	$F_{I\text{-}MMA}$	wt% Iodine	Molecular Weight (g mol^{-1}) $<M_n>$	$<M_w>$
PMMA	0.0	0.0	0.0	310,000	438,000
P(MMA-IMMA$_{2.0}$)	5.9	2.0	7.2	360,000	540,000
P(MMA-IMMA$_{6.9}$)	16.7	6.9	20.5	371,000	589,000
P(MMA-IMMA$_{9.9}$)	23.5	9.9	27.1	374,000	525,000
P(MMA-IMMA$_{11.5}$)	27.1	11.5	29.3	361,000	593,000

Table 2.5 Bead Size of PMMA and P(MMA-IMMA) Copolymer Beads by Suspension Polymerization

Polymer	Bead Diameter (μm)	Bead PDI
PMMA	52 ± 14	0.07
P(MMA-IMMA$_{2.0}$)	54 ± 16	0.09
P(MMA-IMMA$_{6.9}$)	48 ± 15	0.10
P(MMA-IMMA$_{9.9}$)	51 ± 17	0.11
P(MMA-IMMA$_{11.5}$)	56 ± 16	0.08

Table 2.6 Thermal Degradation and Glass Transitions for PMMA and P(MMA-IMMA) Copolymer Beads

Polymer	wt% Iodine	Degradation (°C)		T_g (°C)
		5%	10%	
PMMA	0.0	412	433	103
P(MMA-IMMA$_{2.0}$)	7.2	415	432	102
P(MMA-IMMA$_{6.9}$)	20.5	410	426	104
P(MMA-IMMA$_{9.9}$)	27.1	418	433	106
P(MMA-IMMA$_{11.5}$)	29.3	413	424	106

2.3.4.2 Reaction Kinetics

A study of reaction kinetics was performed on a reaction with an initial feed ratio of f_{IMMA}= 6.9 mol% to further elucidate the copolymerization behavior of MMA and IMMA. The reaction had an overall conversion of 84% (Figure 2.6a), but it is clear that IMMA has a lower rate of conversion and a lower total conversion than MMA (Figure 2.6b). Figure 2.6c shows the feed and copolymer composition ratios. The fraction of monomers in the copolymer, F_{MMA} and F_{IMMA}, indicates that the composition of the polymer stays constant throughout the polymerization, indicating a random structure. The copolymer produced is slightly richer in MMA than the feed ratio, most likely due to the steric bulk of the iodine moieties. It would be expected that as the feed becomes enriched with IMMA ($f_{IMMA}>f_{MMA}$) that the cumulative copolymer ratio would also become enriched with IMMA, but this was not observed. The reaction essentially terminates when 94% of the MMA is consumed with only 35% conversion for the IMMA. Homopolymerization of IMMA is most likely prevented by the steric bulk of the iodine groups, and the unsubstituted MMA monomer spacers are necessary to polymerize the IMMA.

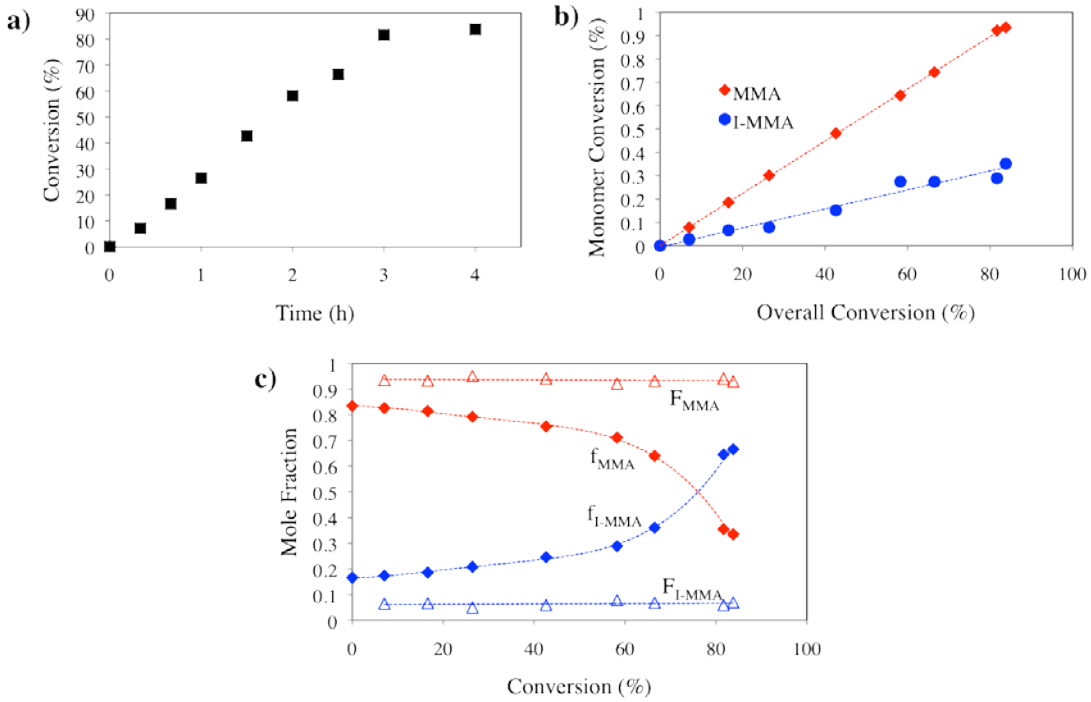

Figure 2.6 Kinetic study of suspension copolymerization of MMA and IMMA. (a) Overall conversion of copolymerization; (b) individual conversion of MMA and IMMA monomers; (c) instantaneous feed ratios of MMA (f_{MMA}) and IMMA (f_{IMMA}) and cumulative copolymer ratios of MMA (F_{MMA}) and IMMA (F_{IMMA}).

2.3.4.3 Iodine Content

The presence of iodine in the beads was confirmed by energy-dispersive X-ray spectroscopy (EDS). For samples with a predicted iodine content of ~20 wt%, it was determined that there was 75 wt% iodine present in the samples. It was also confirmed that radiolucent PMMA contained no iodine. EDS is a good technique to determine the presence of certain elements; however, since it is not always accurate for rough or heterogenous samples, result simply confirms the presence of iodine in the beads and is not a quantitative measurement.

2.3.5 Bone Cement Characterization

Bone cements were formulated with the radiolucent PMMA beads, PMMA beads containing 10 wt% $BaSO_4$ and the radiopaque 20.5 wt% iodine copolymer beads. The powder to liquid ratio was kept constant at 60:40. It is common practice for surgeons to mix $BaSO_4$ with existing commercial bone cements, so a sample containing this inorganic radiopacifying agent was included as a comparison to the synthesized materials.

2.3.5.1 Radiopacity

A CT image of bone cements containing the PMMA beads, the PMMA beads with 10 wt% $BaSO_4$ and the radiopaque 20.5 wt% iodine copolymer beads was taken to determine the comparative radiopacities of the materials. A center slice of the CT image is shown in Figure 2.7a. It is clear that the sample containing the IMMA is more radiopaque than MMA, the sample containing $BaSO_4$ and an aluminum piece of the same dimension. In addition, the radiopacity is more evenly distributed than the sample containing $BaSO_4$ due to the aggregation of the $BaSO_4$ powder. This could be advantageous in monitoring the placement of the cement, as well as trying to detect any cracks or deformations in the cement over time. The Hounsfield units (HUs) were calculated for each sample in Figure 2.7a and displayed in Figure 2.7b. The IMMA sample was more than two times more radiopaque than the $BaSO_4$ sample, and more than four times the radiopacity of unmodified PMMA-based bone cement. The radiopacity of bone is ~2000 HUs, so the wt% iodine could be reduced significantly and still effectively provide contrast to the surrounding material.

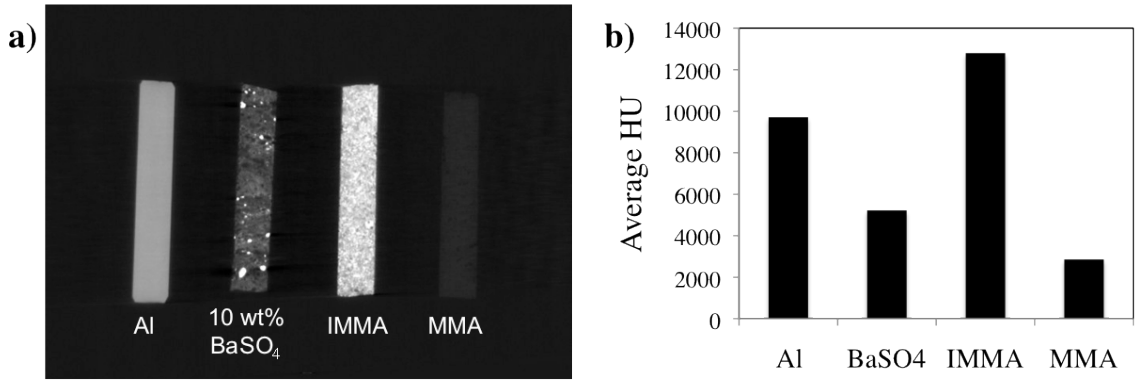

Figure 2.7 Radiopacity of PMMA, P(MMA-*co*-IMMA$_{6.9}$) copolymer and 10 wt% $BaSO_4$ bone cements and an Al control. Dimensions: 2.5 x 0.5 cm cylinder. a) A central slice from the CT image. b) The average Hounsfield units (HU) calculated from the CT images.

2.3.5.2 Compression Testing

Compression testing was preformed on the PMMA, P(MMA-*co*-IMMA$_{8.0}$) copolymer and 10% $BaSO_4$ cements that had been formulated with 60% solids and 40% liquid, the results of which are in Table 2.7. The results are on the same order of magnitude as previous reports of acrylic and iodine-modified bone cements.[23] As expected, the cement reinforced with $BaSO_4$ was of a slightly higher magnitude than the cements without the use of inorganic fillers. The iodine-modified cement, which has 20.5 wt% iodine has approximately the same modulus as the unsubstituted PMMA. In vertebral kyphoplasty applications, higher modulus bone cements are not desirable, as higher modulus cements can cause damage to the surrounding vertebral structures, especially in patients with osteoporosis. The initial results indicate that the functionalized beads do not affect the mechanical properties of the bone cements, making them an attractive alternative to bone cements with inorganic fillers.

Table 2.7 Compression Modulus of Bone Cements

Sample	Modulus, Compression (GPa)
PMMA	1.22 ± 0.04
P(MMA-*co*-IMMA$_{8.0}$)	1.20 ± 0.02
PMMA, 10% $BaSO_4$	1.43 ± 0.14

2.4 Conclusions and Outlook

A novel acrylic monomer was synthesized that can be copolymerized in solution or by suspension with methyl methacrylate. This monomer contains an exceptionally high weight fraction of iodine, and the iodine remains stable thermal and conditions due to the unique structure. Beads of the desired molecular weight (360,000 g mol^{-1}) and diameter (25-50 μm) were targeted in both synthetic schemes. The reaction kinetics for the suspension polymerization determined that monomer addition proceeded in a random fashion, and that the reaction terminated upon the consumption of the MMA due to the steric bulk of the iodinated monomer. The iodinated copolymer beads were formulated into bone cements to make intrinsically radiopaque materials that were imaged by computed X-ray tomography. The copolymer beads showed much higher radiopacity than the radiolucent PMMA, the $BaSO_4$ containing bone cement and the aluminum control. The cements containing the copolymer beads had a comparable modulus to unfunctionalized PMMA, indicating that these materials could be a viable substitute for using inorganic fillers with radiolucent PMMA.

Additional experiments should be performed to further test the compressive strength of these materials with different wt% iodine beads and solid:liquid formulations. It is clear from the CT images that formulations with lower amounts of the iodine monomer could show adequate radiopacity, so more bone cements with lower ratios of iodine should be imaged to determine the optimum ratio of I-MMA that can be incorporated. The stability of the monomer and subsequent copolymers should also be determined in physiological conditions, as well as stability during CT or x-ray imaging. The cytotoxicity of the monomers, the synthesized beads and the formulated bone cements should be performed to determine the *in vivo* viability of these materials.

REFERENCES

(1) Kurtz, S.; Ong, K.; Mowat, F.; Halpern, M. *J. Bone Joint Surg. Am.* **2007**, *89*, 780-785.

(2) Dunne, N. Orthopaedic Bone Cements. CRC Press; 2008.

(3) Department of Research & Scientific Affairs, American Academy of Orthopaedic Surgeons. Annual Incidence of Common Musculoskeletal Procedures and Treatment. www.aaos.org/research/stats/CommonProceduresTreatments-March2014.pdf. March 2014.

(4) Charnley, J. *J. Bone Jt. Surg. (Br)* **1960**, *42-B*, 28-30.

(5) Kuhn, K-D. Bone Cements: Up-to-date Comparison of Physical and Chemical Properties of Commercial Materials. Berlin: Springer-Verlag; 2000.

(6) Lewis, G. *J. Biomed. Mater. Res. Part B* **2008**, *84B*, 301-319.

(7) Lewis, G. *J. Biomed. Mater. Res. Part B* **2006**, *76B*, 456-468.

(8) Kusy, R. P.; *J. Biomed. Mater. Res.* **1978**, *12*, 271-305.

(9) Hass, S. S.; Brauer, G. M.; Dickson, M. A. *J. Bone Joint Surg.* **1975**, *57-A*, 380-391.

(10) Sih, G. C.; Berman, A. T. *J. Biomed. Mater. Res.* **1980**, *14*, 311-316.

(11) Ginebra, M. P.; Albuixech, L.; Fernandez-Barragan, E.; Aparicio, C.; Gil, F. J.; San Roman, J.; Vazquez, B.; Planell, J. A. *Biomaterials* **2002**, *23*, 1873-1882.

(12) Vila, M. M.; Ginebra, M. P.; Gil, F. J.; Planell, J. A. *J. Biomed. Mater. Res. (Appl. Biomat.)* **1999**, *48*, 128-134.

(13) Ginebra, M. P.; Aparicio, L.; Albuixech, L.; Fernandez-Barragan, E.; Gil, F. J.; Planell, J. A. *J. Mater. Sci. Mater. Med.* **1999**, *10*, 733-737.

(14) Topoleski, L. D. T.; Ducheyne, P.; Cuckler, J. M. *J. Biomed. Mater. Res.* **1990**, *24*, 135-159.

(15) Sabokbar, A.; Fujukawa, Y.; Murray, D. W.; Athanasou, N. A. *J. Bone Joint Surg. (Br)* **1997**, *79-B*, 129-134.

(16) Isaac, G. H.; Atkinson, J. R.; Dowson, D.; Kennedy, P. D.; Smith, M. R. *Eng. Med.* **1987**, *16*, 167-173.

(17) Caravia, L.; Dowson, D. Fisher, J.; Jobbins, B. *Proc. Inst. Mech. Eng.* **1990**, *204*, 65-70.

(18) Cooper, J. R.; Dowson, D.; Fisher, J.; Jobbins, B. *J. Med. Eng. Technol.* **1991**, *15*, 63-67.

(19) Kruft, M. A. B.; Benzina, A.; Blezer, R.; Koole, L. H. *Biomaterials*, **1996**, *17*, 1803-1812.

(20) Davy, K. W. M.; Anseau, M. R.; Odlyha, M.; Foster, G. M. *Polym. Inter.* **1997**, *43*, 143-154.

(21) Ginebra, M. P.; Aparicio, C.; Albuixech, L.; Fernandez-Barragan, E.; Gil, F. J.; Planell, J. A.; Morejon, L.; Vazquez, B.; San Roman, J. *J. Mater. Sci. Mater. Med.* **1999**, *10*, 733-737.

(22) van Hooy-Corstjens, C. S. J.; Govaert, L. E.; Spoelstra, A. B.; Bulstra, S. K.; Wetzels, G. M. R.; Koole, L. H. *Biomaterials* **2004**, *25*, 2657-2667.

(23) Boelen, E. J. H.; Lewis, G.; Xu, J.; Slots, T.; Koole, L. H.; van Hooy-Corstjens, C. S. J. *J. Biomed. Mater. Res. Part A* **2008**, *86A*, 76-88.

Chapter III
ENDGROUP FUNCTIONALIZATION OF POLY(ETHYLENE TEREPHTHALATE) DERITIVES WITH UREIDOPYRIMIDINONE

3.1 Introduction

Telechelic endgroups have received a lot of attention for their ability to create reversible supramolecular polymers with properties not accessible by traditional polymerization routes.[1,2] Supramolecular "polymers" can be synthesized by bringing together "monomers" with highly directional, self-assembling non-covalent bonds. Initially, work focused on small molecule monomers, but more recently oligomers, have been end-functionalized to create macromers that can be chain extended via supramolecular chemistry. Endgroup moieties utilizing metal coordination,[3] ionic interactions,[4,5] host-guest complexes[6] or hydrogen-bonding functionalities can be incorporated into directional complementary (A-B) or self-complementary units (A-A) that will assemble into larger polymeric materials. Of these options, hydrogen bonding shows promise because of the sensitivity to external stimuli and because of the availability of large variety of functional groups.[7]

Some of the most simple hydrogen-bonding endgroups are carboxylic acids. In an early study by Lillya *et al.*, poly(THF) oligomers of a variety of molecular weights were polymerized with carboxylic endgroups. They found that the COOH-functionalized materials behaved as elastic materials below the thermal transition attributed to the endgroup dimerization, while the materials without COOH

endgroups behaved as liquids.[8] Recently, more sophisticated directional systems with multiple hydrogen bonds from urethane and urea functionalities have evolved, but one of the most common endgroups utilized to achieve the supramolecular effect is ureidopyrimidinone (UPy) due to the ease of synthesis and a high association constant, $K_{assoc}>10^7$ M^{-1}.[9,10,11] The effectiveness of this group can be attributed to existence of four complementary hydrogen-bonding sites and lateral aggregation of the endgroups.[12,13,14] The direction dimerization behavior of this group is illustrated in Scheme 3.1. The introduction of terminal UPy groups can improve polymer properties concurrent with the increase in effective molecular weight via the self-complementary (A-A) endgroups and the formation of physical crosslinking sites via lateral aggregation.[13,15,16] The resulting supramolecular thermoplastic elastomers are thermally reversible above the dissociation temperature of the UPy groups and exhibit shear thinning in the melt.

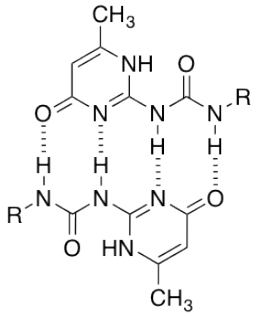

Scheme 3.1 The quadruple hydrogen bonding dimerization of two ureidopyrimidinone (UPy) functionalities.

The structure-property relationships of the UPy endgroup have been extensively studied with low molecular weight, low T_g materials, such as poly(ethylene butylene) (PEB).[9,10,15,16,17] PEB has a low T_g, -57 °C, so that in the absence of the hydrogen-bonding endgroups it remains liquid at room temperature.

When added to the polymer, the UPy endgroup can have a significant effect on the properties of the functionalized materials, resulting in materials that can be processed into films with tensile properties. The strength at which the UPy groups associate, and therefore the virtual molecular weight and modulus of the material, can be tuned by eliminating hydrogen-bonding sites or modifying the length of the aliphatic spacer between the polymer and the isocytosine head.[16] Fibril formation and film morphology is dependant on lateral aggregation and can be affected by the addition of aliphatic R groups on the isocytosine head.[10] While the structure-property relationships of low T_g materials have been well established, investigations probing the effect of the UPy endgroup on high T_g or high T_m materials have been limited.

While low transition temperature materials have a multitude of applications, many engineering and commodity thermoplastics are high T_g or high T_m materials because they have good mechanical characteristics below the thermal transition temperature, and exhibit good flow behavior above the T_g or T_m.[18] Increasing the molecular weight of a polymer will enhance the mechanical characteristics, but will increase melt viscosity, making the material more difficult and more expensive to synthesize and process. Lowering the molecular weight will enable easier processing conditions, but is detrimental to mechanical properties. Ultimately, enhancing the mechanical properties of a low molecular weight material would be ideal, and endgroup functionalization with supramolecular moieties provides a promising route to improving these properties.

In a study by Long and coworkers, polystyrene, a commodity plastic with a T_g~100 °C, was endcapped with a hydrogen bonding endgroup structurally similar to that of the UPy endgroup.[19] The effect of the addition of this endgroup was an 8-20 °C increase in T_g and a 100-fold increase in the melt viscosity in comparison to the hydroxyl endcapped materials. In a prepolymer of 2400 g mol^{-1}, the T_g increased from 72 to 92 °C. In systems where dimerization was determined to be the principal mode of supramolecular enhancement a significant increase in the T_g was not observed. Instead, the increase in the T_g was attributed to the presence of aggregates in the melt. This work did not go on to study the mechanical repercussions of the hydrogen bonding endgroup, but it did show that hydrogen-bonding endgroups have a significant impact on the polymer properties of high T_g plastics.

To investigate the enhancement the mechanical properties of low molecular weight engineering plastics, hydroxyl-terminated poly(butylene terephthalate) (PBT) and poly(butylene isophthalate) (PIT) were endcapped with the UPy moiety.[15] The melt viscosities of the low molecular weight endcapped materials were comparable to the viscosity of unendcapped polymers of the same molecular weight, but the impact strength and elongation at break were comparable to unmodified polymers of higher molecular weights. Despite these results, no enhancement in the tensile modulus for the modified polymers was observed, suggesting that the association mechanism may differ from that of the low T_g materials, but further investigations were not performed.

One of the major drawbacks of hydrogen-bonded supramolecular materials is the high degree of creep that can occur while under load, but it has been suggested that strong interchain interactions and crystalline domains have the potential to prevent creep, and can possibly lead to thermoplastic elastomers with enhanced properties.[1] One genre of polymers that fulfills these requirements is aromatic polyesters. The polyester functionalities in the backbone and π-π stacking amplify interchain interactions, leading to high T_g and high T_m materials. Herein, we investigate the effect of the UPy endgroup on poly(ethylene terephthalate) derivatives modified with cyclohexanedimethanol (CHDM), PETG, of different molecular weights. Hydroxyl-endcapped PETG polymers with molecular weights of 2000, 3800 and 6800 g mol^{-1} were endcapped with the UPy moiety and studied in solution and in films.

3.2 Experimental Methods

3.2.1 Materials

All materials were purchased from Sigma Aldrich, Fisher Scientific or VWR International and used as received unless otherwise noted. Hydroxyl-endcapped glycol-modified PETG polymers (MW=2000, 3800 and 6800 g mol^{-1}) were kindly provided by Eastman Chemical Co. 2(6-Isocyanatohexylaminocarbonylamino)-6-methyl-4[1H]pyrimidinone (MIS) was synthesized according to literature.[10] To remove acidic impurities, chloroform (anhydrous, stabilized with amylenes, Sigma Aldrich) and 1,3,5-trichlorobenzene (anhydrous, Sigma Aldrich) were passed over a basic alumina column and stored over molecular sieves prior to use.

3.2.2 Polymer Characterization

PETG and UPy functionalized polymers were characterized in $CDCl_3$ using a Bruker 600 AVANCE ^1H NMR, TA Instruments Q200 differential scanning calorimeter (DSC) (heating rate=10 °C/min, cooling rate=5 C°/min), Perkin Elmer Pyris 1 TGA (thermogravimetric analyzer) (TGA) (heating rate=5 °C/min), Waters gel permeation chromatography (GPC) system in $CHCl_3$ relative to polystyrene standards, and attenuated total reflectance Fourier transform infrared spectroscopy (ATR-FTIR) using a Bruker ALPHA FT-IR spectrometer.

3.2.3 Film and Solution Characterization

Dynamic Mechanical Analysis to determine the storage modulus at 30 and 100 °C and T_g was performed on a TA Istruments G2 RSA. Strain at yield, strain at break, stress at yield, stress at break and Young's Modulus was determined on an Instron 5566. Viscosity measurements were performed on a TA Instruments G2 ARES.

3.2.4 PETG Modification

Modification of 6.8K PETG. 20.0 g (2.9 mmol, 1 eq.) $PETG_{6.8K}$ was dissolved in 400 mL anhydrous $CHCl_3$ in a dry flask with a reflux condenser, followed by the addition of 2(6-isocyanatohexylaminocarbonylamino)-6-methyl-4[1H]pyrimidinone (MIS) (2.59 g, 8.8 mmol, 3 eq.) and dibutyltin dilaurate (DBTDL, 5 drops) to form a cloudy suspension. The reaction was heated to 65 °C and stirred overnight under N_2. After 18 h, silica gel is added to the reaction with an additional 3 drops of DBTDL and stirred at 65 °C for an additional 2 h. The solution is then hot filtered over sand (sea washed), and the silica gel and sand is washed with additional hot $CHCl_3$. The filtrate is reduced my rotary evaporation and the white solid is dried *in vacuo*

overnight at 90 °C. The product is then cooled to ~78 °C and ground into a powder with a modified coffee grinder and dried *in vacuo* overnight at 100 °C. Yield: 13.65 g (63 %). ^{1}H NMR δ (ppm): 13.10 (s, 1H), 11.81 (s, 1H), 10.11 (s, 1H), 8.09 (s, 4H) 5.81 (s, 1H), 5.07 (s, 1H), 3.23 (bs, 2H), 3.16 (bs, 2H), 2.20 (s, 3H), 1.58 (bs, 2H), 1.35 (bs, 2H).

Modification of 3.8K PETG. The procedure is the same as above, except 11.2 g $PETG_{3.8K}$ was combined with 2.6 g MIS in 250 mL anhydrous $CHCl_3$. Yield 6.56 g (59%).

Modification of 2K PETG. The procedure is the same as above, except 10.0 g $PETG_{2K}$ was combined with 4.4 g MIS in 500 mL anhydrous $CHCl_3$. Yield: 7.16 g (55%).

3.2.5 Solution Film Casting

3.2.5.1 Filtering

1 g of polymer was dissolved in 20 g $CHCl_3$ and filtered through 0.45 μm PTFE filters. The solvent was then removed by rotary evaporation. The polymer was then redissoved in 1,3,5-trichlorobenzene (~25 wt% for PETG, ~13 wt% for functionalized polymers). The solution was warmed to 120 °C and cast onto hot (120 °C) clean glass with a doctor blade. The film was heated to 120 °C for 16 h at ambient pressure. The film was then put under reduced pressure and the temperature was raised to 190 °C for 6 h. To remove the film from the glass, the film was put into a 50-80 °C water bath for several hours until the film came away from the glass easily. The film was dried with a lint-free paper towel.

3.2.5.2 Centrifugation

1 g of polymer was dissolved in 40 mL $CHCl_3$ and centrifuged at 4000 rpm for 1 h. The solution was decanted or pipetted off and then the solvent was removed by rotary evaporation. The polymer was then redissoved in 1,3,5-trichlorobenzene (~25 wt% for PETG, ~13 wt% for functionalized polymers). The solution was warmed to 120 °C and cast onto hot (120 °C) clean glass with a doctor blade. The film was heated to 120 °C for 16 h at ambient pressure. The film was then put under reduced pressure and the temperature was raised to 190 °C for 6 h. To remove the film from the glass, the film was put into a 50-80 °C water bath for several hours until the film came away from the glass easily. The film was dried with a lint-free paper towel.

3.2.6 Tensile Testing

Dynamic Mechanical Analyzer (DMA). Strips of 5 mm width were subjected to a temperature sweep from 25 °C to 120 °C at a heating rate of 3 °C/min with a prestrain of 0.1N axial force, frequency of 1 Hz and a strain of 0.1%.

Instron. Samples with widths of 3 mm were put under a tensile load at a rate of 10 mm/min at room temperature.

3.2.7 Viscosity Testing

The viscosity of the samples were determined utilizing a 50 mm 0.02 radian cone plate at a temperature of 80 °C, an initial shear rate of $5x10^{-5}$ to 50 1/s and a duration of 60s.

3.3 Results and Discussion

3.3.1 Endgroup Modification

The endgroup modification of the PETG polymers was achieved by reacting the isocyanate functionality of the UPy endgroup with the hydroxyl endgroups of PETG polymer in solution (Scheme 3.2). This synthetic method is well established for polymers such as PEB,[10] but Long and coworkers utilized a bulk reactive extrusion method in their work with aromatic polyesters, PIT and PBT.[15] To remove the excess endgroup, silica gel was added and the unreacted isocyanate reacted with the hydroxyl functionalities on the surface of the silica gel. Removal of the silica gel was initially performed by vacuum filtration over paper, but it was found that this method insufficiently removed the silica gel, so filtering over a sand column was adopted.

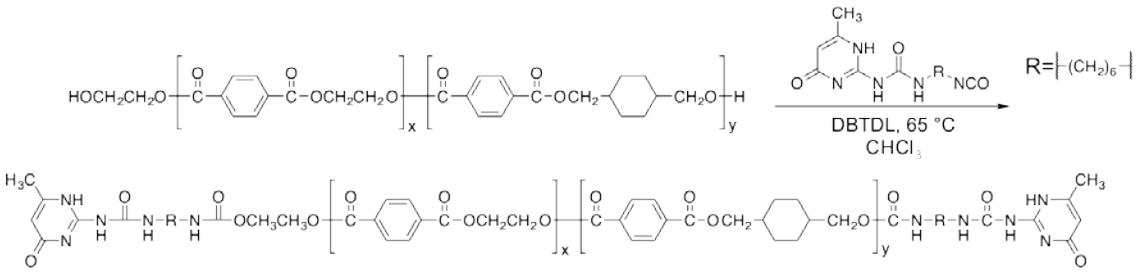

Scheme 3.2 Reaction of hydroxyl-endcapped PETG polymers in solution with UPy endgroup functionality.

3.3.2 Chemical Characterization

Post-functionalization, the polymers were analyzed by ^{1}H NMR, ATR-FTIR, GPC and TGA to confirm the attachment of the UPy functionality. $PETG_{2K}$ was used to confirm attachment since the high concentration of endgroups enabled easy visualization. The ^{1}H NMR (Figure 3.1) after purification has peaks that indicate the

presence of the UPy endgroups. Integrations of the UPy endgroup peaks and the aromatic peak of the PETG indicate full functionalization of the PETG polymers. The appearance of the peak at 3.23 ppm also indicates reaction of the isocyanate group with a hydroxyl functionality to form an adjacent urethane moiety.

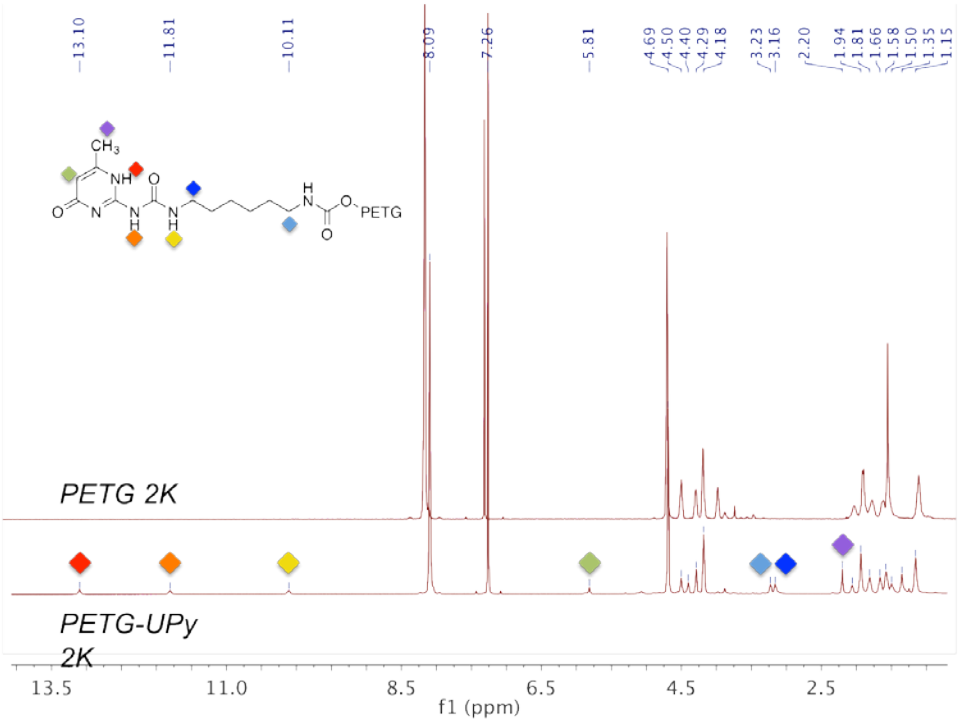

Figure 3.1 ^{1}H NMR in $CDCl_3$ of the PETG polymer (top) and the UPy-functionalized PETG polymer (bottom). Peaks indicating the presence of the UPy endgroup are labeled.

ATR-FTIR of $PETG_{2K}$, the UPy endgroup and the purified $PETG_{2K}$-UPy further confirm attachment of the UPy functionality. In the full spectrum in Figure 3.2a, the disappearance of the peak ~3500 cm^{-1} after reaction of the PETG with the UPy endgroup indicates the reaction of the hydroxyl groups. There is also no remaining isocyanate functionality in the final product, which can be visualized at ~2200 cm^{-1} in the spectrum of the endgroup. In the $PETG_{2K}$-UPy spectrum in Figure 3.2b, the

appearance of the amide I and II bands at 1660 and 1580 cm^{-1} as well as the appearance of a peak at 1510 cm^{-1} attributable to a secondary amine indicate the presence of the UPy endgroup in the product.

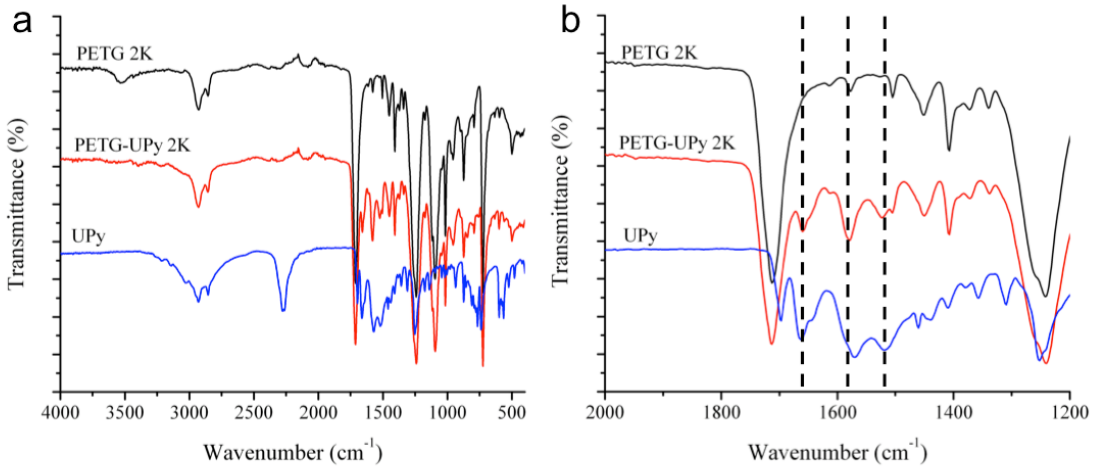

Figure 3.2 The ATR-FTIR of the $PETG_{2K}$, $PETG_{2K}$-UPy and UPy endgroup. a) Full spectrum, and b) inset from 2000-1200 cm^{-1}.

3.3.3 Molecular Weight

A slight increase in molecular weight for all samples was detected by GPC post-functionalization (Figure 3.3). The increase in molecular weight is due to the additional weight of the endgroup, and also to aggregation of the endgroups. Using a lower concentration of sample could prevent aggregation, but lower concentrations were unable to be resolved from the baseline. The large peak at ~10.5 min in the $PETG_{2K}$-UPy spectrum indicates the presence of excess UPy endgroup. This was resolved by modifying the work up of the polymer by improving the filtration of the product. The molecular weights and PDIs are listed in Table 3.1. The reduction in PDI and the increase in molecular weights after functionalization indicate that some lower molecular weight chains have been lost

in the purification. This could be due to the affinity of the UPy endgroup to silica gel, which has been observed previously, and some of the lower molecular weight fractions may remain with the silica gel after filtering. This could be an additional explanation for the observed increase in the molecular weight.

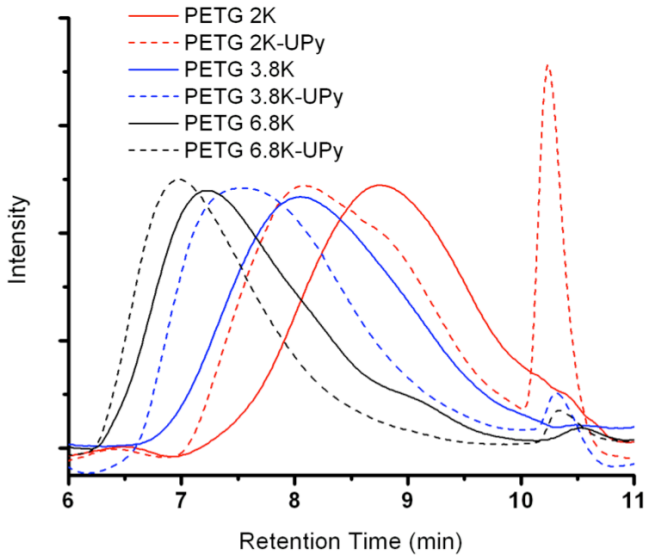

Figure 3.3 GPC traces of the PETG polymers and the polymers post-functionalization.

Table 3.1 Molecular Weights of PETG and PETG-UPy Polymers

Sample	M_n (g mol^{-1})[a]	M_w (g mol^{-1})[a]	PDI[a]
$PETG_{2K}$	3150	5520	1.75
$PETG_{3.8K}$	6100	10200	1.68
$PETG_{6.8K}$	11800	21000	1.78
$PETG_{2K}$-UPy	6010	9020	1.50
$PETG_{3.8K}$-UPy	10200	16500	1.61
$PETG_{6.8K}$-UPy	17100	27400	1.60

[a] Determined by GPC in THF using polystyrene standards.

3.3.4 Thermal Degradation

Onset of thermal degradation of the UPy endgroup has been reported to occur at 250 °C, and thermal degradation can verify the presence of the UPy

functionality on the polymer chain. In Figure 3.4, the functionalized and unfunctionalized materials were degraded in air by TGA, and it is clear that the onset of degradation of the functionalized materials is at lower temperatures than the unfunctionalized counterparts, indicating the presence of an additional functionality. Typically, UPy functionalized materials show a step loss at 250 °C due to the loss of the isocytosine head, but this behavior was not observed in these materials. This may be because the backbone of the PETG prepolymer is more thermally stable than the previously used low-T_g polymer backbones. Table 3.2 shows the 5% degradation temperatures for the unfunctionalized PETG in addition to the functionalized materials before and after processing into films. As expected, the 5% degradation temperatures for the functionalized materials before and after processing into films are lower than the unfunctionalized polymers. Upon processing into films, the functionalized materials show an increase in the degradation temperatures in comparison to the bulk materials, indicating the presence of solvent in the materials before heating to 190 °C.

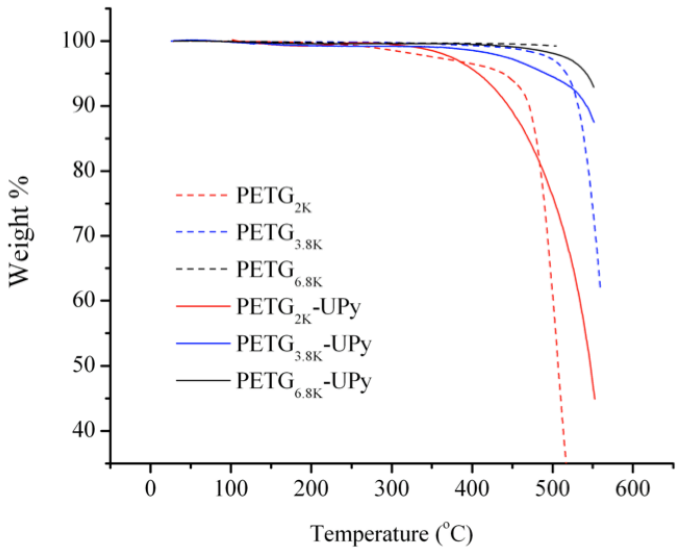

Figure 3.4 Thermal gravimetric analysis (TGA) traces in air of the functionalized and unfunctionalized PETG polymers. PETG materials were degraded from the bulk material, and the functionalized materials degraded after processing into films at 190 °C.

Table 3.2 Thermal Degradation of PETG and PETG-UPy Polymers

Sample	$T_{5\%}$ (°C)[a]	$T_{5\%}$ (°C)[b]
$PETG_{2K}$	439	nd
$PETG_{3.8K}$	520	nd
$PETG_{6.8K}$	--	nd
$PETG_{2K}$-UPy	379	407
$PETG_{3.8K}$-UPy	503	492
$PETG_{6.8K}$-UPy	528	542

[a] Bulk material [b] after processing into films at 190 °C

3.3.5 Thermal Transitions

Upon functionalization of the PETG with the UPy endgroup, we would expect the glass transition temperature to remain the same, or increase slightly. After drying the bulk material at 120 °C, a 5-10 °C depression in the T_g was observed (Table 3.3). This can be attributed to a plasticizing effect from a small amount of solvent remaining in synthesized materials. Upon casting the materials into thin films and drying at 190 °C *in vacuo*, the T_g of the functionalized materials increased dramatically to values higher than the comparable unfunctionalized materials. This increase could be attributed to the presence of the UPy functionalities. This is theory is supported by the fact that the lower molecular weight materials saw the greatest increase in T_g, as the shorter chain lengths will be more affected by the constraint of the endgroups and the concentration of the UPy functionalities is the highest. The films can be dissolved into solution after processing, so crosslinking of the materials is not a likely reason for the observed increase in T_g. To further

confirm that the increase in the T_g is due to the endgroup functionalities and is not a artifact of processing, the PETG films should processed in the same manner.

Table 3.3 Glass Transition Temperatures of PETG and PETG-UPy Polymers

Sample	T_g (°C)[a]	T_g (°C)[b]
$PETG_{2K}$	41.9	nd
$PETG_{3.8K}$	59.6	nd
$PETG_{6.8K}$	71.2	nd
$PETG_{2K}$-UPy	35.3	63.0
$PETG_{3.8K}$-UPy	47.9	73.6
$PETG_{6.8K}$-UPy	60.2	79.4

[a] Bulk material [b] after processing into films at 190 °C

Initially, films were cast from 1,3,5-trichlorobenzene and heated to 120 °C under vacuum to remove solvent. DSC traces of these materials, shown in Figure 3.5, revealed a melting temperature around 150 °C on the first heat. A dissociation temperature is characteristic for UPy functionalized materials, although the dissociation temperature for UPy functionalized PEB is usually at 80 °C. This melting temperature was not visible for the unfunctionalized materials and so it is possible that the melting event can be attributed to the dissociation of the UPy endgroups. It is also possible that the melting event is due to the crystallinity of the PETG backbone, and residual solvent in the system could induce crystallization. It would also be expected that the lower molecular weight sample would have a larger ΔH_m due to the lack of chain entanglements. The ΔH_m for the $PETG_{3.8K}$-UPy was greater than the $PETG_{6.8K}$-UPy, which can be attributed to either the larger concentration of hydrogen-bonding endgroups, or the greater crystallinity of the lower molecular weight material due to a lack of chain entanglements.

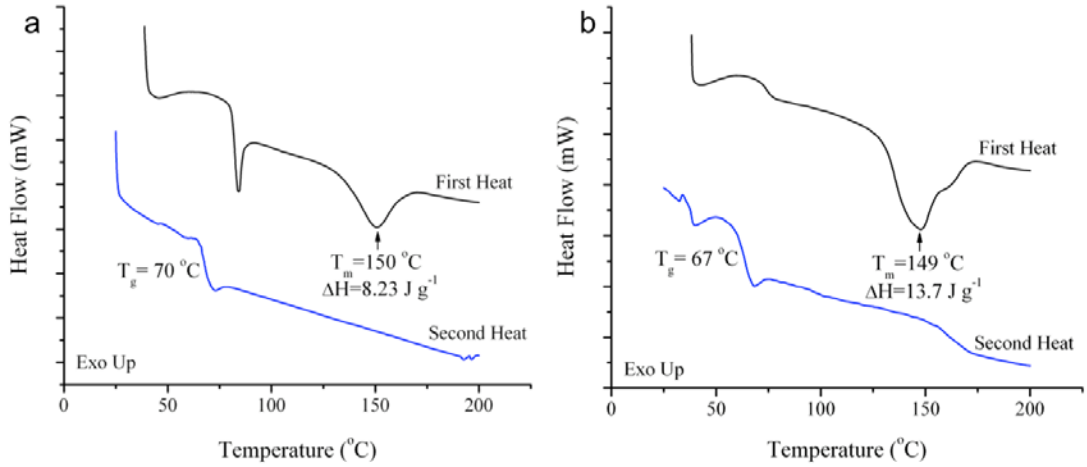

Figure 3.5 DSC traces of the first and second heats of $PETG_{6.8K}$-UPy (a) and $PETG_{3.8K}$-UPy (b) after heating to 120 °C.

When films were annealed to 190 °C to remove residual haziness, no melting temperature was observed in the first or second heats of the DSC traces, as seen in Figure 3.6. Since the UPy dissociation temperature is most commonly observed at 80 °C, it seems likely that the melting temperatures observed in Figure 3.5 are due to crystallization of PETG. The glass transition temperatures elevated 6–9 °C after processing into films, indicating the loss of residual solvent upon heating the films to 190 °C, so the melting temperatures in Figure 3.5 are most likely solvent-induced crystallization of the PETG backbone.

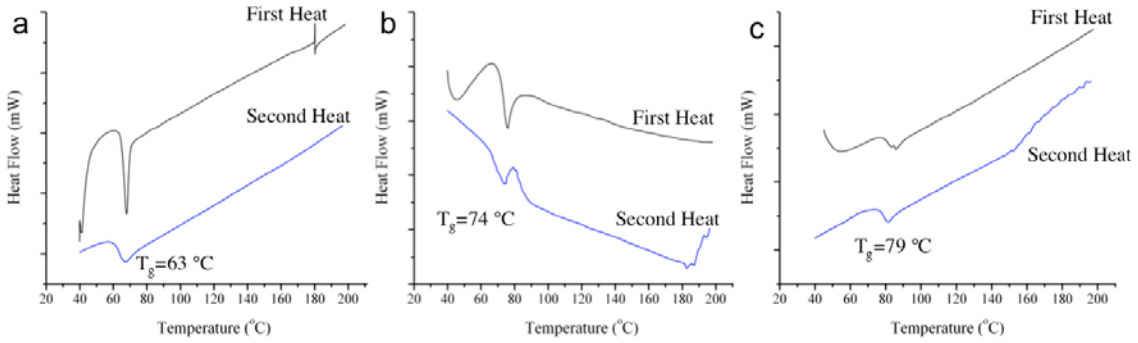

Figure 3.6 DSC traces of the first and second heats of $PETG_{2K}$-UPy (a), $PETG_{3.8K}$-UPy (b) and $PETG_{6.8K}$-UPy (c) after heating the films to 190 °C.

3.3.6 Viscosity

The viscosity of $PETG_{6.8K}$ and $PETG_{6.8K}$-UPy were determined in 2.5-12.5 wt% solutions of 1,3,5-trichlorobenzene at 80 °C (Figure 3.7). The maximum viscosity of the $PETG_{6.8K}$ solution is less than 0.1 Pa•s (Figure 3.7a), while the functionalized polymer gives much greater viscosities, with a maximum viscosity for the same concentration of solution around 5 Pa•s (Figure 3.7b). An increase in viscosity was observed for other UPy-endcapped materials, and is attributed to the increase in virtual molecular weight due to the end-to-end association and physical crosslinking due to the lateral aggregation of the endgroups. It is also possible that the endgroups are interacting with the ester functionalities along the backbone of the polymer, which could increase interchain interactions and the number of physical crosslinks, thus increasing the viscosity.

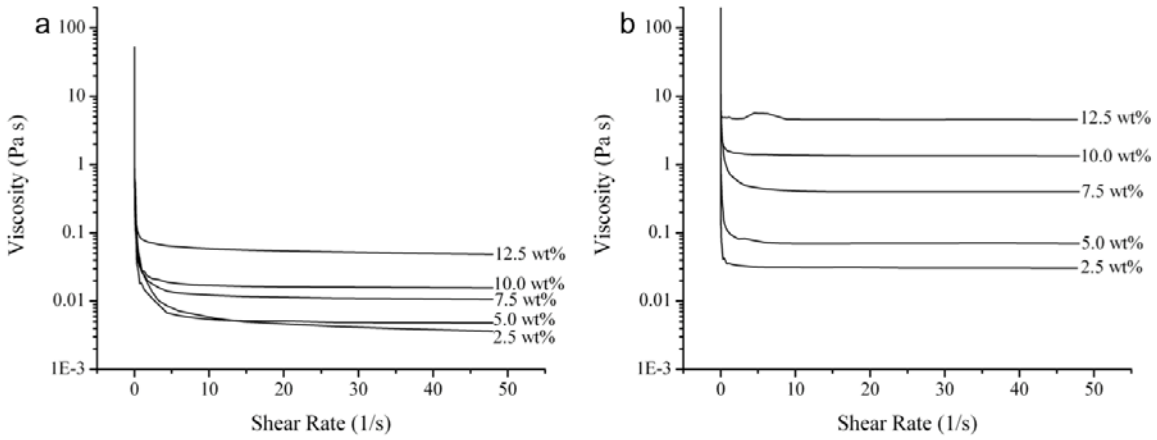

Figure 3.7 Viscosity of 2.5–12.5 wt% solutions in 1,3,5-trichlorobenzene of $PETG_{6.8K}$ (a) and $PETG_{6.8K}$-UPy (b). Shear rates from $5x10^{-5}$–50 1/s at a temperature of 80 °C.

3.3.7 Film Formation and Tensile Testing

The materials were processed into films via a solution casting method from 1,3,5-trichlorobenzene. Two different purification methods of the casting solution were employed. In the first method, the polymers were centrifuged from chloroform and then cast from trichlorobenzene after removal of the chloroform by rotary evaporation. In the second method, the polymers were dissolved in chloroform and filtered through a 0.45 μm filter, after which the chloroform was removed by rotary evaporation. The polymers were redissolved in trichlorobenzene and cast into films. The solutions were not filtered from trichlorobenzene as the solutions were too viscous to pass through the filter. While filtration provided a more homogenous film due to the removal of small particulates, it was not a feasible method for the 2K and 3.8K functionalized polymers. This is presumably because the UPy endgroups in solution create aggregates that are too large in size to pass through the filter with ease. The films were dried uncovered at 120 °C until they

were no longer tacky, followed by drying at 190 °C *in vacuo* to remove any remaining solvent and to remove any residual haziness due to crystallization.

Dynamic mechanical analysis (DMA) was performed to determine the T_g the materials after being processed into films. The glass transition temperatures of the films determined by DMA are higher by 6-16 °C than the glass transition temperatures determined for the films by DSC, as seen in Table 3.3 and Figure 3.6. Increasing the molecular weight of the unfiltered materials caused a slight increase in T_g, as expected. A greater increase in molecular weight was observed when the transition temperatures were determined by DSC (Table 3.3). The discrepancy between the DMA and DSC data is most likely due to the effect of the heating rate in the DSC. For $PETG_{6.8K}$ and $PETG_{6.8K}$-UPy films that had been filtered prior to film casting (Table 3.4), it was determined that the T_g remained approximately the same, as would be expected. The addition of a telechelic endgroup should not significantly change the T_g significantly high molecular weight polymer because the restriction of the polymer chain ends should not affect the backbone segmental motion of the majority of the polymer chain.

The cold and hot storage moduli, E', were measured using DMA in a tensile geometry (Table 3.4). The filtered $PETG_{6.8K}$ sample had a slightly higher E'_{cold} than the filtered $PETG_{6.8K}$-UPy sample, while the E'_{hot} was slightly lower. Filtering of the functionalized materials was more difficult than the unmodified PETG, indicating that a significant fraction of the chains are being removed from the UPy-functionalized material. The removal of the more crystalline, low molecular weight chains could result in a lower E'_{cold}, while interactions of the UPy group by

intermittent hydrogen bonding in the melt and an overall increase in average molecular weight could increase the E'_{hot}. As the molecular weight of the UPy modified materials increases, there is a decrease in the E'_{cold}. This is indicative of decreasing crystalline character with increasing molecular weight. The higher crystallinity of the lower molecular weight materials, as well as the higher concentration of hydrogen bonding endgroups likely contributes to this behavior. Conversely, as the molecular weight of the prepolymer increases, the E'_{hot} also increases, presumably due to the increased polymer chain length and number of entanglements in the melt. Overall, this data indicates that the UPy functionalization does not significantly alter the properties of the $PETG_{6.8K}$ materials, and the functionalized materials follow the same trend that would be expected for unfunctionalized PETG materials. Determination of the moduli of the $PETG_{2K}$ and $PETG_{3.8K}$ will further elucidate the effect of endgroup functionalization on these materials.

Table 3.4 Glass Transition Temperatures and Storage Moduli of PETG and PETG-UPy Films

Sample	T_g (°C)[a]	E'_{cold} (GPa)[b]	E'_{hot} (MPa)[c]
$PETG_{2K}$-Upy	79.3 ± 0.1	1.1 ± 0.07	1.7 ± 0.3
$PETG_{3.8K}$-Upy	81.9 ± 0.3	0.94 ± 0.09	2.3 ± 0.7
$PETG_{6.8K}$-Upy	85.1 ± 0.3	0.69 ± 0.06	3.1 ± 0.2
$PETG_{6.8K}$-Upy*	82.5 ± 0.3	0.90 ± 0.40	5.0 ± 0.1
$PETG_{6.8K}$*	82.4 ± 0.4	1.2 ± 0.3	4.6 ± 0.4

*filtered
[a] Determined by tanδ of DMA [b] measured at 30 °C [c] measured at 100 °C

While the stress and strain at yield and Young's Modulus did not change significantly with functionalization or molecular weight, significant differences in the strain at break were observed. Comparing $PETG_{6.8K}$ to $PETG_{6.8K}$-UPy in Table 3.5, there is an increase in the strain at break due to the more ductile nature of the modified materials, enhanced by the presence of hydrogen bonding groups. Comparing the functionalized materials of different molecular weights allows us to examine the interplay between molecular weight and endgroup concentration. Higher molecular weight materials will increase the strain at break due to the longer chains and the number of entanglements, while a higher concentration of endgroups will increase the number of non-covalent interactions between the chains and the chain ends. The $PETG_{3.8K}$-UPy sample has the highest strain at break, while the unfiltered $PETG_{6.8K}$-UPy has the lowest. The $PETG_{3.8K}$ sample is most likely showing the highest maximum strain because the trade-off between molecular weight and endgroup concentration has been optimized. It is expected that the $PETG_{2K}$-UPy sample would have a lower strain at break than the $PETG_{6.8K}$-UPy due to the increased number of entanglements for a higher molecular weight material, as seen in the filtered $PETG_{6.8K}$-UPy material. Therefore, the low strain at break of the unfiltered $PETG_{6.8K}$-UPy sample is most likely due to poor film quality, making the true properties comparable to the filtered sample.

Table 3.5 Tensile Properties of PETG and PETG-UPy Films

Sample	Stress at Yield (MPa)	Strain at Yield (mm/mm)	Stress at Break (MPa)	Strain at Break (mm/mm)	Young's Modulus (MPa)
$PETG_{2K}$-Upy	48 ± 14	0.14 ± 0.03	44 ± 14	6.4 ± 1.2	560 ± 260
$PETG_{3.8K}$-Upy	43 ± 5	0.09 ± 0.01	54 ± 6	8.5 ± 1.3	720 ± 50
$PETG_{6.8K}$-Upy	40 ± 10	0.10 ± 0.03	33 ± 9	3.2 ± 1.9	680 ± 150
$PETG_{6.8K}$-Upy*	39 ± 2	0.10 ± 0.02	48 ± 4	6.6 ± 0.5	740 ± 40
$PETG_{6.8K}$*	39 ± 6	0.10 ± 0.04	45 ± 11	5.9 ± 1.5	830 ± 110

*filtered

3.4 Conclusions and Outlook

The solution-phase reaction of 2K, 3.8K and 6.8K PETG with an isocyanate-functionalized ureidopyrimidinone has yielded difunctionalized UPy-terminal aromatic polyesters of three different molecular weights. The reaction has been confirmed by NMR, ATR-FTIR, GPC, TGA and DSC. Both NMR and ATR-FTIR indicate that there has been complete substitution of the endgroups. The UPy-functionalized materials display moderate supramolecular properties both in solution and in films. In solution, the viscosity of functionalized $PETG_{6.8K}$-UPy is approximately 100x higher than the unfunctionalized counterpart. In films processed at 190 °C, an increase in the strain at break was observed for the functionalized materials, and the $PETG_{3.8K}$-UPy film showed the highest strain at break, indicating that the 3.8K material has the optimal molecular weight and endgroup concentration to maximize the supramolecular effect.

To further characterize the materials that have been synthesized, it would be advantageous to process the materials into films in the melt. In this way, the effect of solvent and small particulates will be eliminated, giving more reproducible results. Additionally, the UPy groups may behave differently in the melt than they

do in solution and give different properties. If the materials can be processed in the melt, melt rheology will elucidate the aggregation behavior and the melt viscosity.

To further study the structure-property relationships, the PETG prepolymers can be reacted with different endgroups containing the isocytasine head. To synthesize different endgroups, 4-amino-4-hydroxy-6-methylpyrimidine can be reacted with different diisocyanates. The different diisocyanates could lead to endgroups with different degradation pathways and dissociation constants, which should change the thermal and tensile properties of the materials. Ideally, an endgroup that dissociates at a higher temperature than the existing UPy functionality could be used to maximize the supramolecular effect of the endcapped aromatic polyesters. Since the 3.8K materials were found to display the largest effect upon functionalization, using only this prepolymer going forward would be a judicious use of resources while still being able to determine the relationships desired. The same chemical, thermal, tensile and rheological characterization should be completed for the new materials, in addition to NMR studies to determine the dissociation constants.

REFERENCES

(1) Brunsveld, L.; Folmer, B. J. B.; Meijer, E. W.; Sijbesma, R. P. *Chem. Rev.* **2001**, *101*, 4071–4097.

(2) De Greef, T. F. A.; Smulders, M. M. J.; Wolffs, M.; Schenning, A. P. H. J.; Sijbesma, R. P.; Meijer, E. W. *Chem. Rev.* **2009**, *109*, 5687–5754.

(3) Li, H.; Wu, L. *Soft Matter* **2014**, *10*, 9038–9053.

(4) Craig, S. L. *Angew. Chem. Int. Ed.* **2009**, *48*, 2645–2647.

(5) Faul, C. F. J.; Antonietti, M. *Adv. Mater.* **2003**, *15*, 673–683.

(6) Dong, S.; Zheng, B.; Wang, F.; Huang, F. *Acc. Chem. Res.* **2014**, *47*, 1982–1994.

(7) Bertrand, A.; Lortie, F.; Bernard, J. *Macromol. Rapid Comm.* **2012**, *33*, 2062–2091.

(8) Lillya, C. P.; Baker, R. J.; Hutte, S.; Winter, H. H.; Lin, Y.-G.; Shi, J.; Dickinson, L. C.; Chien, J. C. W. *Macromolecules* **1992**, *25*, 2076–2080.

(9) Keizer, H. M.; van Kessel, R.; Sijbesma, R. P.; Meijer, E. W. *Polymer* **2003**, *44*, 5505–5511.

(10) Folmer, B.; Sijbesma, R. P.; Versteegen, R. M.; van der Rijt, J.; Meijer, E. W. *Adv. Mater.* **2000**, *12*, 874–878.

(11) Sijbesma, R. P.; Meijer, E. W. *Chem. Commun.* **2003**, 5–16.

(12) Beijer, F. H.; Sijbesma, R. P.; Kooijman, H.; Spek, A. L.; Meijer, E. W. *J. Am. Chem. Soc.* **1998**, *120*, 6761–6769.

(13) Van Beek, D. J. M.; Spiering, A. J. H.; Peters, G. W. M.; te Nijenhuis, K.; Sijbesma, R. P. *Macromolecules* **2007**, *40*, 8464–8475.

(14) Botterhuis, N. E.; van Beek, D. J. M.; van Gemert, G. M. L.; Bosman, A. W.; Sijbesma, R.P. *J. Poly. Chem. Part A* **2008**, *46*, 3877–3885.

(15) Yamauchi, K.; Kanomata, A.; Inoue, T.; Long, T. E. *Macromolecules* **2004**, *37*, 3519–3522.

(16) Kautz, H.; van Beek, D. J. M.; Sijbesma, R. P.; Meijer, E. W. *Macromolecules* **2006**, *39*, 4265–4267.

(17) Heinzmann, C.; Coulibaly, S.; Roulin, A.; Fiore, G. L.; Weder, C. *ACS Appl. Mater. Interfaces* **2014**, *6*, 4713–4719.

(18) Kellener, P. G. *Adv. Polym. Technol.* **1990**, *10*, 219-230.

(19) Yamauchi, K.; Lizotte, J. R.; Hercules, D. M.; Vergne, M. J.; Long, T. E. *J. Am. Chem. Soc.* **2002**, *124*, 8599-8604.

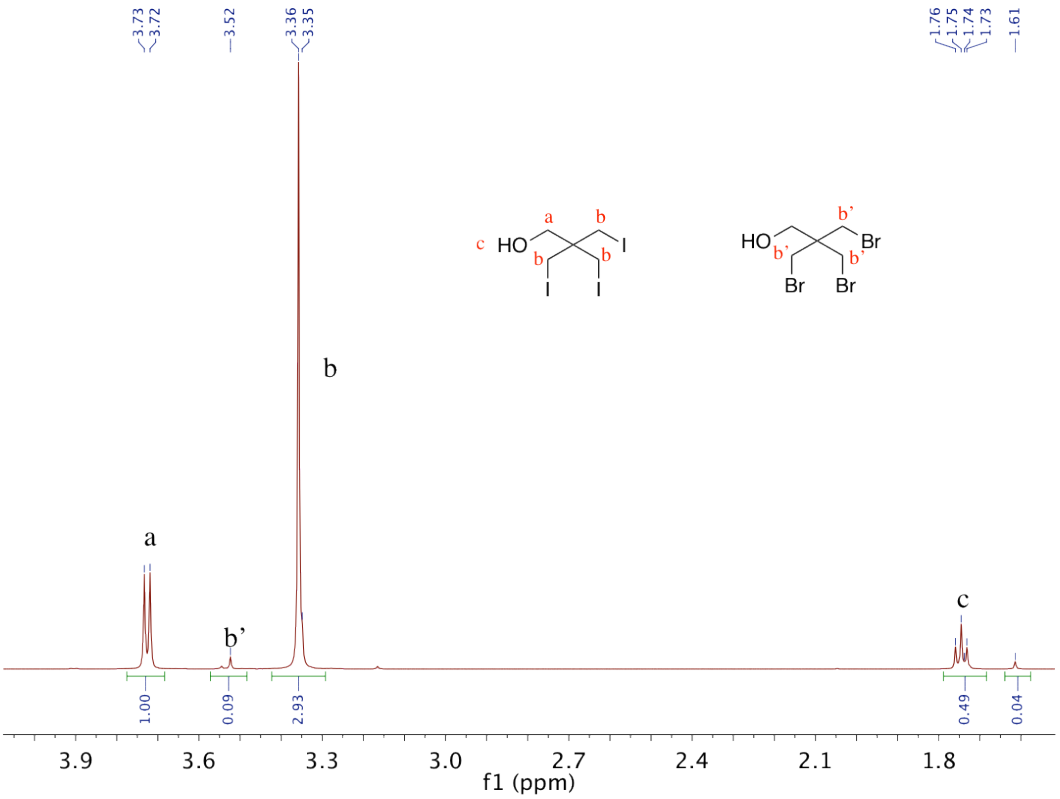

Figure S1 ^{1}H NMR of 3-iodo-2,2-bis(iodomethyl)propanol in $CDCl_3$.

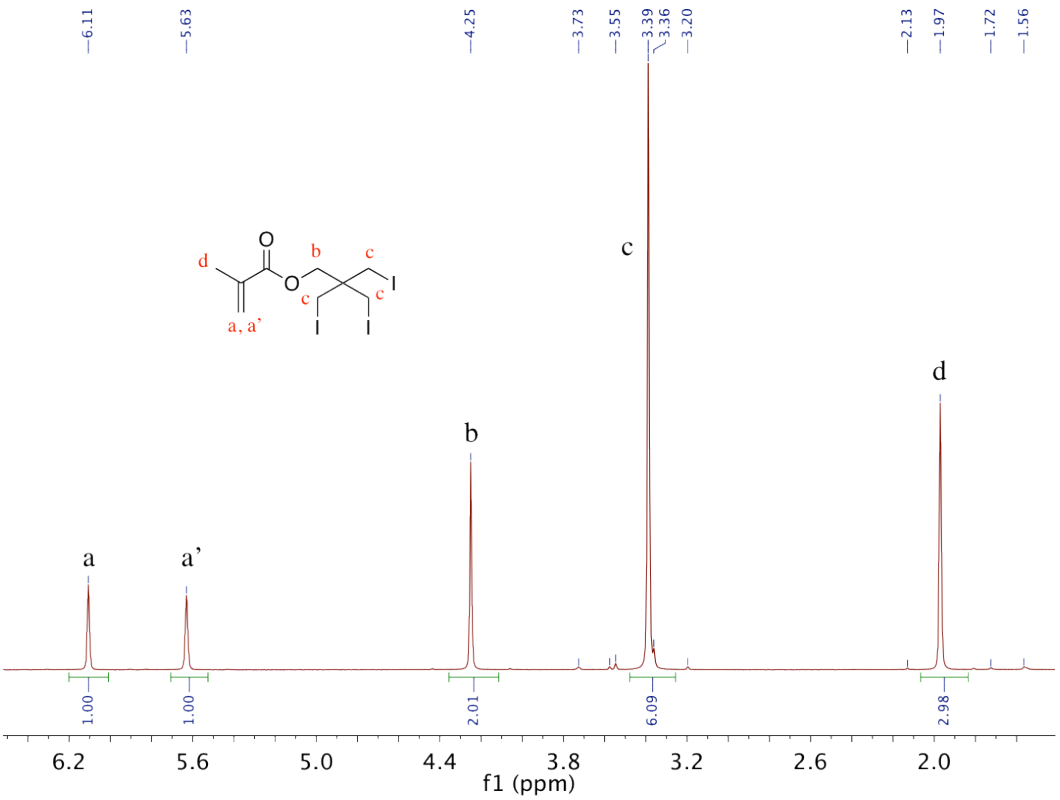

Figure S2 ^{1}H NMR of 3-iodo-2,2-bis(iodomethyl)propyl methacrylate (IMMA) in $CDCl_3$.

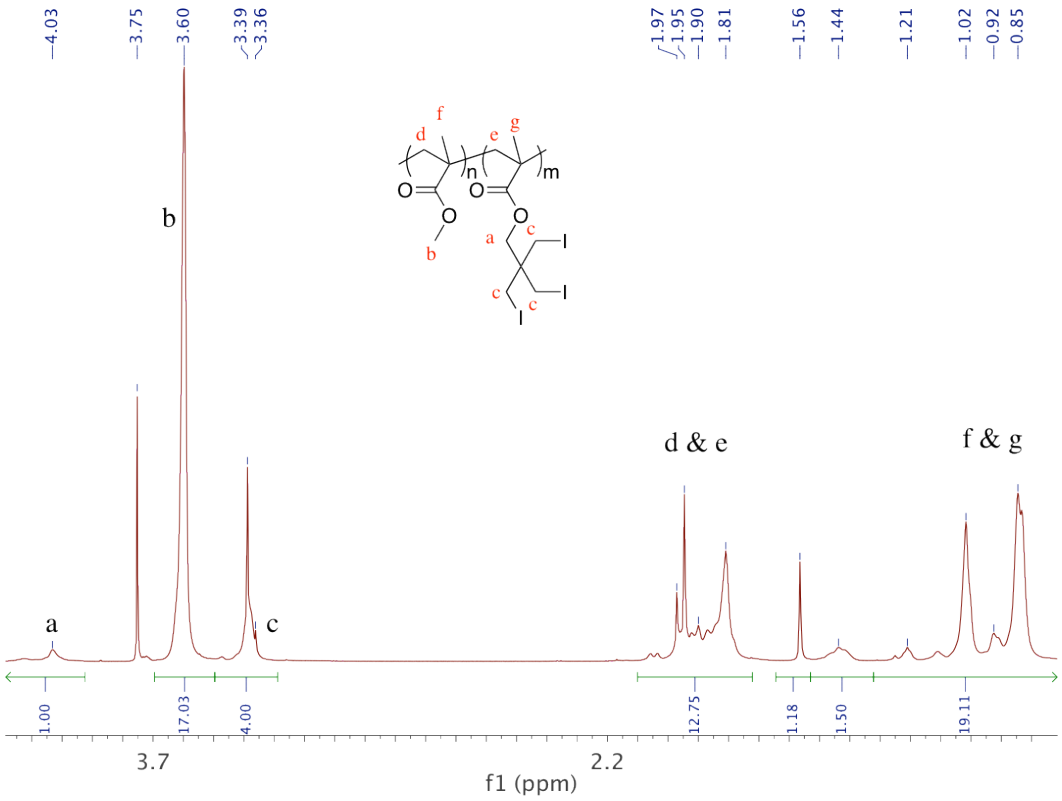

Figure S3 ^{1}H NMR of poly(MMA-IMMA$_{6.9}$) copolymer polymerized by suspension in $CDCl_3$.